4-4-2023

SNOW DISTRIBUTION AND INFLUENCE IN TAYLOR VALLEY, ANTARCTICA, USING REMOTE SENSING

Katherine McNulty
Louisiana State University and Agricultural and Mechanical College

Peter Doran
Louisiana State University at Baton Rouge

Mark Salvatore
Northern Arizona University

Suniti Karunatillake
Louisiana State University at Baton Rouge

SNOW DISTRIBUTION AND INFLUENCE IN TAYLOR VALLEY, ANTARCTICA, USING REMOTE SENSING

A Thesis

Submitted to the Graduate Faculty of the
Louisiana State University and
the Agricultural and Mechanical College
in partial fulfillment of the
requirements for the degree of
Master of Science

in

The Department of Geology and Geophysics

by
Katherine McNulty
BS, University of Cincinnati, 2016
MS, May, 2023

This thesis is dedicated to my family,
especially my mom, for always encouraging me to pursue my dreams,
and my furry office assistants- Rud and Little Booty Judy

Acknowledgments

I am funded as a graduate and teaching assistant by the Geology and Geophysics Department John Franks Fund at Louisiana State University. This research is funded by the National Science Foundation Grant #OPP1637708 for Long Term Ecological Research. I would like to thank my advisor Peter Doran, and my committee members Mark Salvatore and Suniti Karunatillake, for their generous support and guidance. I would like to acknowledge the support of the 2021-2022 field team and science support personnel that made this possible. I would like the thank Anna Wright, Abby Jackson, Mia Vanderwilt, and Emily Reynebeau for helping with sample collection; and my lab mates Michael Stone and Krista Myers.

Table of Contents

Acknowledgments xiv

Table of Contents 11

List of Tables 13

List of Figures 14

Abbreviations 15

Abstract 16

Chapter 1. Introduction 17

Chapter 2. Background 20
2.1. Previous Snow Studies 20
2.2. Basin Descriptions 21

Chapter 3. Methods 23
3.1. Satellite Data 23
3.2. Determining In Situ Validation Locations from Satellite Data 23
3.4. Area Volume Calculations 24
3.5. Analyzing the Historic Record 27
3.6. Basin Calibration 29

Chapter 4. Results 31
4.1 Satellite Coverage Analysis 31
4.2. Snow Volume Calculations 32
4.3. Basin Calculations 35
4.4. SWE Budgets through time 36

Chapter 5. Discussion 44
5.1 Ground Truth Area vs Volume Work 44
5.2 TV Coverage Through Time 45
5.3 Spatial Variability 46
5.4 Late Season Variability 47

Chapter 6. Conclusions 49

Appendix A. Python Program for Calculating Snow Area from Satellite Images..50

Appendix B. Additional Figures.....54

References.....65

Vita.....69

List of Tables

1. Basin Bounds 22

2. Monthly early season average snow area in TV and sub-basins. 41

3. Monthly early season average SWE in TV and sub-basins 42

4. Early season averages from 2004 to 2022 43

5. Late season averages from 2004 to 2022 43

List of Figures

1. Displays the Three Major Dry Valleys of the MDV 17

2.Basin Descriptions 22

3. Sampling Density Cutter 25

4. Single-Point Sampling Schematic 26

5. Contour Schematic.....27

6. Flow Chart 29

7. Historic Frequency of Coverage 32

8. Grid Volume Contours 33

9. Area Volume Model 35

10. Classification Scheme 37

11. Basin Area to Quadrat Area Relationship 38

12. Basin Volume to Volume area relationship 38

13.Histroic Snow Area by Basin.....39

14. Historic Fractional Coverage by Basin.....40

15. Range of Historic Snow Coverage 41

Abbreviations

ArcGIS Pro	Arc Geographical Information System Pro software
AMPS	Antarctic Mesoscale Prediction System
ASL	Amundsen Sea Low
AWS	Automated Weather System
MCM LTER	McMurdo Long Term Ecological Research
MDVs	McMurdo Dry Valleys
NSF	US National Science Foundation
PGC	Polar Geospatial Center
SWE	Snow Water Equivalent
TV	Taylor Valley

Abstract

The McMurdo Dry Valleys is the largest ice-free area in Antarctica, but seasonal snow covers the valley floors sporadically throughout the year. In this study, a model to estimate areal snow coverage from satellite imagery was created. An area-volume model was created to estimate the amount of snow water equivalent (SWE) from the snow area extracted from the imagery. Snow cover influences the total albedo, the hydrologic budget, and the soil moisture and soil temperature in Taylor Valley (TV). Quantifying snow precipitation in TV is challenging because snow redistributes with winds, sublimates, or melts within a short period. Previous estimates found the amount of snow precipitation in TV is small, less than 100 mm/a. (SWE); even so, snow cover may influence processes in the valley. To better understand the controls and feedbacks of snow cover in the valley, a long-term record of spatially distributed abundance is required. This research creates a long-term record of snow cover data in TV using satellite images. The area of snowpacks was calculated by creating a classification scheme based on the brightness of panchromatic images. During the 2021-2022 field season, 250 m x 250 m sampling quadrats were surveyed to approximate how area and volume relate to SWE. Volumetric SWE was calculated by measuring in situ the length, width, depth, and density of each snowpack in the quadrat. There is a strong relationship between the area and the volume of the snowpacks (R^2=0.942, P=0.182). With this information, estimates of the SWE can be made from the area calculated from satellite imagery. The average snow area for the entire extent of TV in late winter/early summer (September-December) from 2004 to 2022 is 65.26 km^2, the average SWE is 0.0310 km^3, and the average SWE depth is 75.72 mm. The amount of areal snow coverage is important when calculating the energy balance of TV, as well as understanding the availability of soil moisture to the soil ecosystem year-to-year. The available SWE can also influence seasonal surface and subsurface hydrology. While most precipitated snow in TV will sublimate or be redistributed by the wind, it is important to quantify how much snow has accumulated each season, especially with a warming climate, which could drastically influence snow accumulation and dynamics in TV.

Chapter 1. Introduction

The McMurdo Dry Valleys (MDVs) make up the largest ice-free region in Antarctica and are classified as a polar desert (Levy, 2013). The MDVs are situated within the Transantarctic Mountains in southern Victoria Land (*Figure 1*). Taylor Valley (TV) is the southernmost of the larger MDVs, where the average annual air temperature at the valley bottom is -15°C to -30°C, the annual snow water equivalent (SWE) is 3 to 100 mm, and the annual surface radiation varies between 72 and 122 W m^{-2} (Obryk et al., 2020; Fountain et al., 2010; Fountain et al., 1999). Within TV, there are three major glaciers: Taylor Glacier is an outlet glacier plugging the western margin of TV, while Canada and Commonwealth are mountain glaciers that drain to the south into TV from the Asgard Range. The valley also contains three large lakes: Lake Bonney (which is separated into east and west basins, or lobes), Lake Hoare, and Lake Fryxell. The valley terminates to the east at McMurdo Sound.

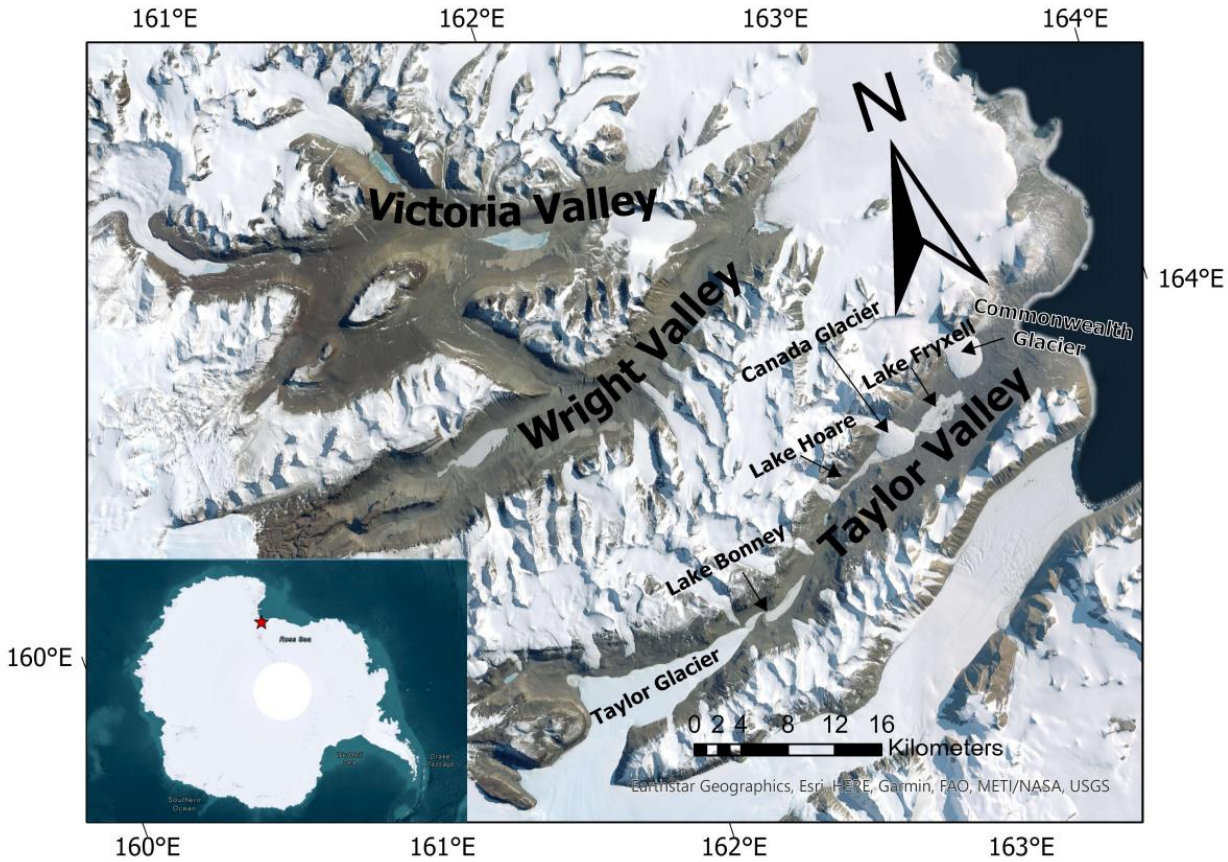

Figure 1. Map displays the three major Dry Valleys of the MDV. Taylor Valley (TV) is the southernmost valley, terminating into the Ross Sea. The three major glaciers in TV are: Taylor Glacier, Canada Glacier, and Commonwealth Glacier. The three major permanently ice-covered lakes in TV are: Lake Bonney (east and west lobes), Lake Hoare, and Lake Fryxell.

The US National Science Foundation (NSF) founded the McMurdo Dry Valleys Long-Term Ecological Research (MCM LTER) site in 1992. The MCM LTER is one of 28 LTER sites worldwide (https://lternet.edu/). The goal of the LTER network is to conduct long-term field observations and experiments so that current and future generations can better understand complex ecosystems and identify factors that cause widespread changes in those ecosystems. The MCM LTER group presently collects long-term records on the following general landscape units: glaciers, lakes, meteorology, soils, and streams. Since 1994, snow accumulation measurements are collected every fifteen minutes at four automated weather stations (AWS) in TV. The measurements have been collected using a combination of Campbell Scientific SR50 Sonic Ranging Sensors, Belfort weighing buckets, and Texas Electronics TE525MM antifreeze tipping buckets. Nevertheless, snowfall estimates from AWS do not relate well to snow on the ground (Myers et al., 2022). The snow that does not sublimate or melt soon after it falls is redistributed and redeposited by the wind as patchy snowpacks across the landscape that can vary in shape, size, volume, density, and other fundamental properties (Fountain et al., 1999).

Snow is important to the MDV ecosystem for four main reasons: 1) it influences the energy balance through its effect on albedo, 2) it restricts photosynthetically active radiation from reaching the soil subsurface (e.g. reducing photosynthesis beneath lake ice), 3) it serves as a source of soil moisture and 4) it contributes to stream flow.

The increase in albedo can reduce or fully eliminate the amount of energy input into the valley floor from solar radiation (Bergstrom et al., 2020; Dana et al., 1998; Fountain et al., 1999). The total effective surface albedo in TV is known to greatly affect the timing and amount of melt generated in a season (Bergstrom et al., 2020). Glacial snow cover during the summer months is the most influential aspect of a glacier's energy balance; this is because the summer months are when the glacier is most susceptible to melt, which is mainly driven by the absorption of solar radiation (Fountain et al.; 1999; Fountain et al.; 2006; Fountain et al., 2010). On glaciers, snow accumulation can increase albedo by up to 20%, thus reducing the amount of melt and streamflow produced by the glacier (Bergstrom et al., 2020; Dana et al., 1998; Fountain et al., 1999). However, there is a positive relationship between the amount of snow accumulation at the terminus of the glaciers, and the amount of early spring melt (Fountain et al., 1998; Fountain et al.,1999), indicating that early season snowfall greatly influences the amount of liquid water generated each season. While snow is clearly an important contributor to the MDV ecosystem, current methods cannot determine the influence of instantaneous snow cover on the valley water and energy budgets.

Quantifying snow cover may also aid in improving the hydrologic model of the valley. Snow accumulation on the valley bottom is thought to influence permafrost formation and perseverance (Fountain et al., 2010; Hagedorn et al., 2007; Sugden et al., 1995). Both dry and ice-cemented permafrost are influenced by snow cover distribution, as snow acts to preserve permafrost and replenish the active layer (Hagedorn et al., 2007). Seasonal melting of permafrost in the valley has been shown to feed some ephemeral streams and increase soil moisture, so less snow presence over time may result in higher rates of permafrost melt (McKay et al., 1998). During anomalous decadal warming events, permafrost melt has been shown to have a greater influence on valley hydrology (Harris et al., 2007). Some permafrost features in the valley have been hypothesized to be over 6,000 years old, and it is unknown how significant the depletion of relict permafrost deposits in the valley would affect other physical and biological processes in the valley (Denton and Marchant, 2000; Stuiver et al., 1981).

The ephemeral streams in the valley are fed by snowmelt and permafrost melt and

contribute to lake inputs (McKay et al., 1998; McKnight et al., 1999). Snow cover on the lakes reduces photosynthetically active radiation (PAR) and inhibits photosynthesis in the water column (Myers, 2019) and it is hypothesized that snow cover on the valley floor would have similar effects on primary productivity in the soils. While previous studies have examined the influence snow cover has on the glaciers, permafrost, streams, and lakes (e.g. Bertler et al., 2004; Chinn, 1981; Dana et al., 1998; Fountain et al., 1998; Fountain et al., 1999; Fountain et al., 2006; Fountain et al., 2010; McKay et al., 1998; McKnight et al., 1999; Myers, 2019; Sugden et al., 1995; Withrow et al., 2006), the distribution of snow on the valley bottom and its potential role in influencing soil productivity has been understudied (Eveland et al., 2013). Overall, it is known that snow can influence many dynamic processes in TV, so it is imperative to have a baseline dataset. Therefore, with a warming climate, it must be understood how the total snow coverage in TV is changing.

Measuring snowpack accumulation is very challenging to quantify using only field-based measurements due to the trace amounts that are deposited during any given snow event, the unpredictable manner in which the wind can redistribute snow across the landscape, and that the large study area makes it impossible to manually verify all snowpack estimates. High-resolution satellite imagery provides a valuable tool in the spatial and temporal investigation of snow as it is possible to watch the evolution of the size and spectral properties of the snow as time progresses. This project uses satellite imagery to measure areal snow coverage and estimate snow water equivalent (SWE) volume in TV to augment point measurements of snow accumulation. Having a robust long-term record of snow cover in the valley creates a baseline for snow coverage in the valley and can be used to understand the evolution of the surface hydrology of the MDV in the context of a warming climate.

This study uses field and satellite data to create: 1) a snowpack area-to-volume relationship, 2) a basin to 250 m x 250 m subsampling calibration standard, and 3) an accurate snow coverage baseline dataset for TV. This study implements a more systematic approach to further support ground-based snowpack observations and increase spatial resolution, using high-resolution satellite imagery. Satellite imagery provides a reliable tool for predicting future trends in the distribution, accumulation, and persistence of snow in TV. This new long-term record will be maintained by the MCM LTER group to monitor changes in snowpack area, volume, and SWE.

Chapter 2. Background

2.1. Previous Snow Studies

Snow cover distribution in the valley is primarily controlled by two major factors – the meteorologic occurrence of dry foehn winds and the topographic structure known as Nussbaum Riegel (Fountain et al., 1999; Fountain et al., 2010). A foehn wind is the result of a 'precipitation shadow'; it is the dry dense air that creates adiabatic warming on the lee side of a mountain after the precipitation has dropped from that air mass on the windward side of the mountain. In TV, the foehn winds increase local air temperatures and are characterized by high wind speeds in the down-valley direction due to density differentials of the air masses (Fountain et al., 1999; Nylen et al., 2004; Speirs et al., 2010). The foehn winds can come either from the northern Asgard Range or from the southern Kukri Hills; winds coming from the ice sheet do not deposit much snow in TV (Fountain et al., 2010; Fountain et al., 2016; Kimura, 2007; Myers et al., 2022; Obryk et al., 2020). Foehn winds increase erosion, sublimation, and redistribution of snow (Fountain et al., 2010). The Nussbaum Riegel, a prominent topographic rise south of Lake Hoare, creates a physical barrier and precipitation shadow that prevents snow-producing clouds from progressing from westward eastern basins, Explorers Cove, Fryxell, and Hoare, to the eastern basins, East and West Lobe Bonney (Fountain et al., 2010).

The historical distribution of snow on the valley bottom shows a gradient of decreasing precipitation while moving westward in the valley (Fountain et al., 2010). During the winter, the persistence of snow on the valley bottom in the eastern portion of the valley is greater than during the summer (Fountain et al., 2010). In the western portion of the valley, there is no seasonal variability observed (Fountain et al., 2010; Nylen et al., 2004). The position of the sea ice does not influence the amount of snow cover in the valley but small changes in the Southern Annular Mode (SAM) are likely to influence the meteorological properties in the valley (Fountain et al., 2010; Fountain et al., 2016; Kimura, 2007; Patterson et al., 2005). However, micro-topographic features ranging from 1- 100 m, can greatly influence the persistence of snowpacks in TV (Eveland et al., 2013).

Fountain et al. (2010) created a model to simulate the spatial distribution of snow on the valley floor for one year, from September 2006–August 2007. This model uses measured precipitation data and the Antarctic Mesoscale Prediction System (AMPS) numerical model. Precipitation data were collected from eleven precipitation gauges (weighing buckets and ultrasonic rangers). The AMPS model was created by the US Antarctic Program and incorporates data from surface stations, radiosondes, satellite-derived cloud track winds, sea ice data, and LANDSAT 8 data (Powers et al., 2003). Due to the low amount of precipitation in Taylor Valley, many snow patches are smaller than the 15-meter point-spread resolution of LANDSAT 8. While the Fountain et al. (2010) model is useful, it tends to overestimate the amount of precipitation in the valley and has a spatial resolution that is insufficient for localized valley studies. Standard field methods used for measurements of snowfall accumulation are challenging in this environment due to the sparse nature of snow accumulation. Using high-resolution satellite imagery can provide a new method for establishing a long-term record of snow distribution in TV and can allow us to develop consistent measurement techniques looking back into the past and well into the future as more data continue to be collected.

Myers et al. (2022) found TV receives an average of 1 to 58 mm SWE using data collected from the AWS and a stationary camera at Lake Hoare. This total estimate is very similar to the 3 to 50 mm SWE estimate from Obryk et al. (2020)'s work. Myers et al. (2022)

found SWE was increasing 3 mm/a from 1995 until 2009, and from 2009 until 2017 the SWE was decreasing 1mm/a. There is an observed trend that when there is high spring snow accumulation in the Explorers Cove basin, the Bonney Basins receive more snow accumulation in the summer months (Myers et al., 2022). In the Hoare basin, snow persistence has been increasing by an average of 1 day/a in the fall season. While the data show SWE decreasing in TV, Patterson et al. (2005) suggest with increased moisture availability from the Ross Sea, certain changes in air mass may result in an increase in SWE in TV.

Since 2005 there has been a decrease in the air temperature in all five basins (Obryk et al., 2020) and since 2007 there has been a decrease in snowfall measurements from 3 mm to 1 mm (Myers et al., 2022). Rain is expected to increase in the area with warming conditions. Rain-on-snow events are known to increase melt rates of snowpacks (Cohen et al., 2015). With the anthropogenic induced changing climate, it is critical to know the volume of snow present in the valley to know the maximum potential snow-generated melt.

2.2. Basin Descriptions

The hydrologic setting and topographic divides determine the bounds of the five basins used in this study (*Figure 2*, *Table 1*). The West Lobe Bonney basin is hydrologically dominated by Taylor Glacier and the west lobe of Lake Bonney. The East Lobe Bonney basin is hydrologically influenced by the east lobe of Lake Bonney and is topographically separated by Bonney Riegel to the west and Nussbaum Riegel to the east. Lake Hoare and Canada Glacier heavily affect the hydrology in the Hoare basin. The Fryxell basin is hydrologically controlled by Lake Fryxell and Canada Glacier and is separated from the Hoare basin by Canada Glacier. The Explorers Cove Basin is dominated by the Ross Sea influence and is separated by a topographic high on the western portion of the basin.

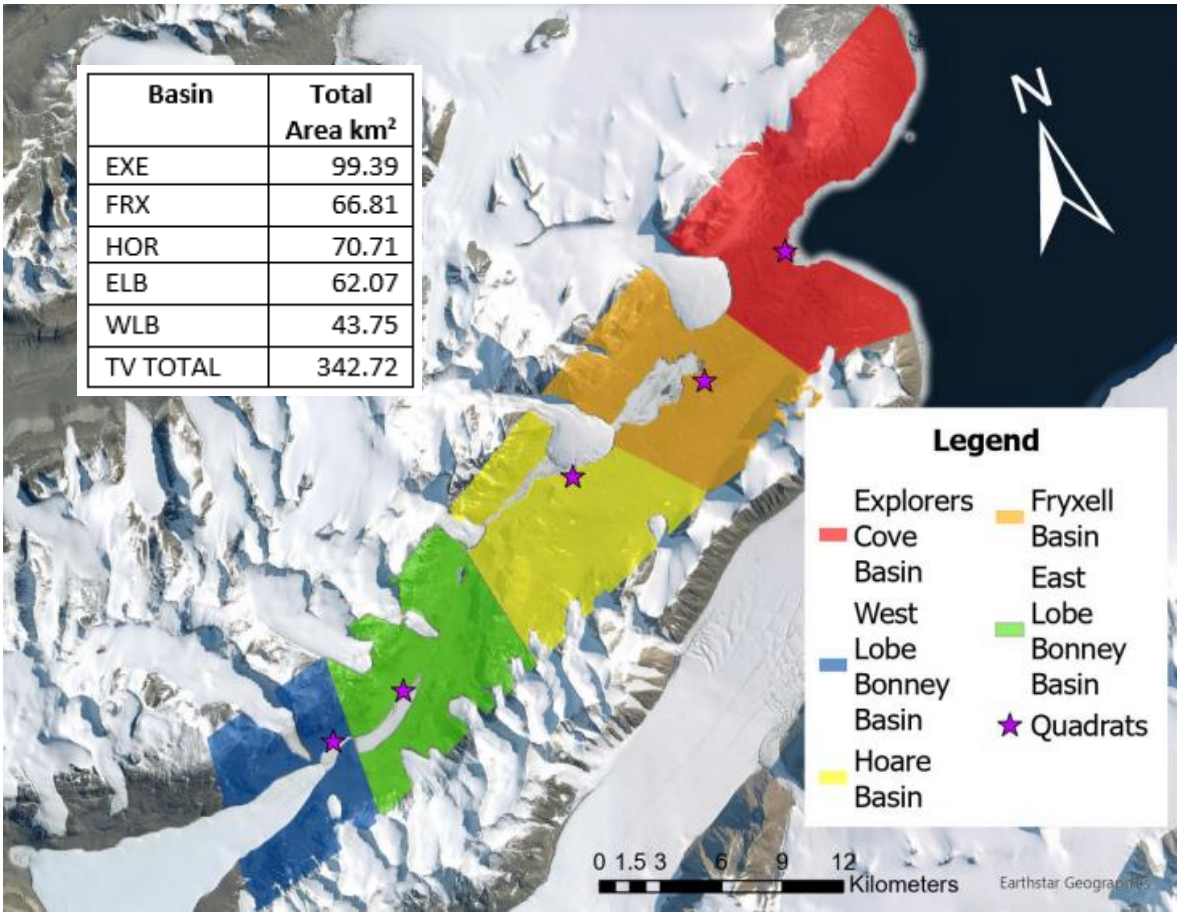

Figure 2. The five basins are displayed here. The 250 m x 250 m quadrats are displayed by the purple stars. Calculated basin areas do not include the glaciers or permanently ice-covered lakes in the valley. The base map image was acquired by Esri, DigitalGlobe, GeoEye, i-cubed, USDA FSA, USGS, AEX, Getmapping, Aerogrid, IGN, IGP, swisstopo, and the GIS User Community.

Table 1. The corner boundaries of the sub-basins in TV. The northwest bound of Explorers Cove basin and the northeast bound of Fryxell basin is below Commonwealth Glacier, and the northwest bound of Fryxell basin, and the northeast bound of Hoare basin is below Canada Glacier.

Basin Name	Northeast	Northwest	Southeast	Southwest
Explorers Cove	77.47378°S	77.58649°S	77.61826°S	77.62331°S
	163.80459°E	163.33931°E	163.69862°E	163.47003°E
Fryxell	77.58649°S	77.62738°S	77.62331°S	77.65935°S
	163.33931°E	163.04299°E	163.47003°E	163.19942°E
Hoare	77.62738°S	77.649443°S	77.65935°S	77.70955°S
	163.04299°E	162.68519°E	163.19942°E	162.76105°E
East Lobe	77.64944°S	77.67852°S	77.70955°S	77.75039°S
Bonney	162.68519°E	162.34746°E	162.76105°E	162.35694°E
West Lobe	77.67852°S	77.69618°S	77.75039°S	77.77547°S
Bonney	162.34746°E	162.06658°E	162.35694°E	162.05651°E

Chapter 3. Methods

3.1. Satellite Data

The imagery used in this study comes from the satellites QuickBird-2, WorldView-2, and WorldView-3 which are operated by DigitalGlobe. QuickBird-2 was deployed in 2001, WorldView-2 was deployed in 2009, and WorldView-3 was deployed in 2014. The QuickBird-2 mission ended in 2014, while both WorldView-2 and WorldView-3 continue to collect data over the MDV. The images used for this study were collected from 2004 until 2022; the images acquired from 2001-2003 were spatially limited and did not cover the study areas.

All satellite data were acquired from the NSF-supported Polar Geospatial Center (PGC) which, through a cooperative agreement with the National Geospatial-Intelligence Agency (NGA), receives, processes, and stores high-resolution commercial and private imagery for use by funded investigators. Data in this study consist exclusively of panchromatic images, which use broadband visible/near-infrared (VNIR) reflectance data to generate grayscale images at sub-meter spatial resolution. Panchromatic images are preferred for this study because the reflectance data is used to identify snow, the brightest natural material that is widespread across the surface, versus the dark barren ground surface. Another reason panchromatic images are preferred compared to multispectral images, is because the higher resolution images will detect smaller snowpacks and provide better estimates for snow area coverage. The panchromatic satellite data were acquired from the PGC as 8-bit digital numbers (DN) to minimize file size and to ensure comparability and compatibility between current, past, and future datasets. 8-bit data are appropriate given the significant difference in albedo between snow-covered surfaces and most other natural surfaces throughout the MDV. Data were projected over Taylor Valley using a Polar Stereographic projection and the WGS 84 datum.

3.2. Determining In Situ Validation Locations from Satellite Data

To validate the snow area to the satellite imagery, and to build a relationship between snow area and snow volume; 250 m x 250 m sampling quadrats were created. These sampling quadrats are useful to estimate total basin coverage, because full-basin coverage is rare and the quadrats are a manageable sampling area. To locate the areas in TV with the historically best cloud-free satellite image coverage, a coverage density map was created using ArcGIS Pro. The density map excluded oblique images, and images with more than 10% cloud cover. Each raster was converted to a polygon for efficiency, then an overlay analysis of the polygons was performed to determine the areas with the highest percentage of coverage. The 2014 LiDAR (Light Detection and Ranging) digital elevation model (DEM) of the valley (Fountain, 2017) was used to verify that the quadrats are located at similar elevations to eliminate biases of altitude effect. The quadrats are located relatively close to a basecamp to make future ground-truthing easier. Using the spatial join analysis in ArcGIS Pro, the 250 m x 250 m quadrats were selected using these three parameters, a high percentage of historical coverage, similar elevation, and proximity to basecamps. To accurately quantify the amount of snow within each quadrat, ground-truthing methods were performed during the 2021-2022 field season. Within each quadrat, all the present snowpacks were sampled by the “single-point method” and one snowpack was sampled using the “grid method.” The single-point snowpacks are assumed to be ellipse shaped, based on field observations. For each single-point snowpack, the GPS locations of the long and wide axes for each snowpack were recorded, using a Garmin InReach (3 m resolution, 95%). The long axis and wide axis of the snowpack were also measured with a field

measuring tape. The depth of each snowpack was sampled at the intersection of the two length measurements, due to the assumption the snowpacks are elliptical in shape. At each depth measurement, at least three snow density measurements were collected. The number of density measurements was dependent on the size of the snowpack. Larger snowpacks required more snow density measurements, to ensure density does not change with depth and to ensure there are no layers present in the snowpacks. The snow density measurements were collected with either 250 or 1000 cm^3 snow density cutters, the size of the cutter was dependent on the size of the snowpack (*Figure 3*); smaller snowpacks often were not large enough to use the 1000 cm^3 cutter.

The grid snowpacks were sampled by taking the GPS track of the perimeter of the snowpack, using a Garmin InReach. Within each grid snowpack, multiple transects were sampled to create a grid pattern. Like the single-point measurements, the depth and density were sampled at each intersection of the various transects. In addition to the standard depth and density measurements, separate snow water equivalent (SWE) samples were collected to determine the amount of debris in the snowpacks. The amount of debris in the samples was calculated by weighing the total sample, evaporating all the water in the sample by heating, then weighing the remaining debris. The SWE is calculated by using Equation 1,

$$SWE = \frac{SD}{WD}V \qquad (1)$$

where SD is snow density, WD is water density and V is snowpack volume. The WD is used in the liquid water phase, in accordance with standard SWE measurements.

3.4. Area Volume Calculations

The volume of each snowpack was calculated from the field area, depth, and density data. The single-point area measurements were calculated by assuming the shape of the snowpacks was elliptical (*Figure 4*) and using Equation 2,

$$A = \pi ab \qquad (2)$$

where *a* is the semi-major axis and *b* is the semi-minor axis. The volumes were calculated using Equation 3,

$$V = 4/3\pi abc \qquad (3)$$

where *c* is the depth of the snowpack. This models the snow pack volume as half of an ellipsoid, treating the pack as exclusively above the plane of the landscape (*Figure 4*).

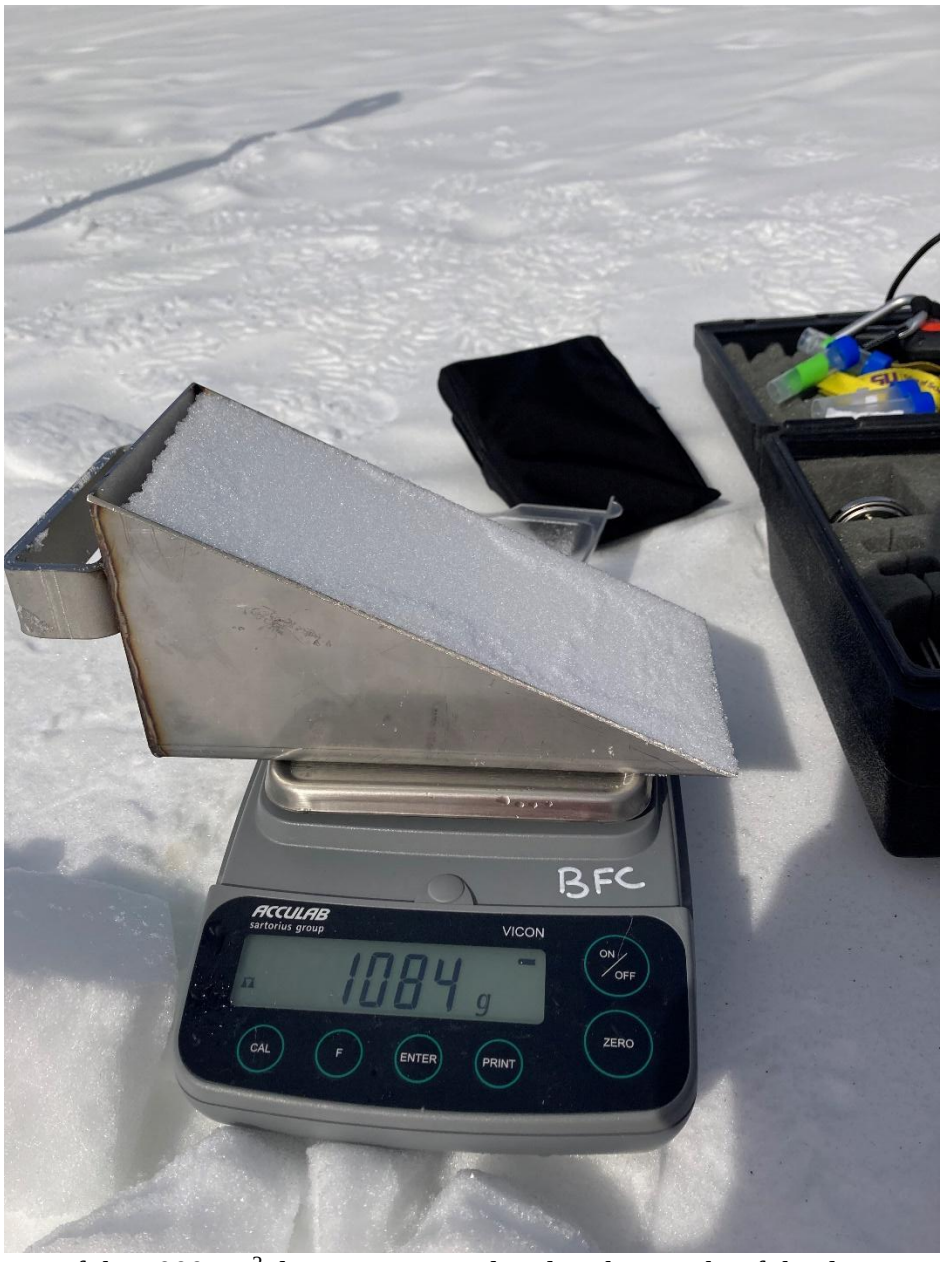

Figure 3. Image of the 1000 cm^3 density cutter and scale. The weight of the density cutter was measured and subtracted from the total weight of the snow density sample and cutter. Each snowpack had a minimum of 3 density measurements.

The grid snowpack areas and volumes were calculated using the "cut and weigh" approach. This analog method uses an electronic analytical balance (in this case a Hanchen BSM220.4, readability 0.1mg, accuracy ±0.1mg) and cardstock to weigh the standard and the complex snowpack shapes. The standard is a scaled 1 m x 1 m square on cardstock that was weighed to find the relationship between a known area, 1 m x 1 m, and the weight of the cardstock. The planar areas of the snowpacks were cut out and weighed, compared to the standard (*Equation 4*). To estimate the volume of each snowpack, 2 cm contour lines were created using the transects and intersection data points from the grid snowpack (*Figure 5*). Each contour line was weighed as an individual planar surface. Each 2 cm interval had a unique

geometry. Each 2 cm intervals from the perimeter of the snowpack to the thickest portion of the snowpack were weighed to determine each 2 cm interval area.

$$Area\ of\ snowpack = Weight\ of\ Snowpack\left(\frac{Area\ of\ Standard}{Weight\ of\ Standard}\right) \qquad (4)$$

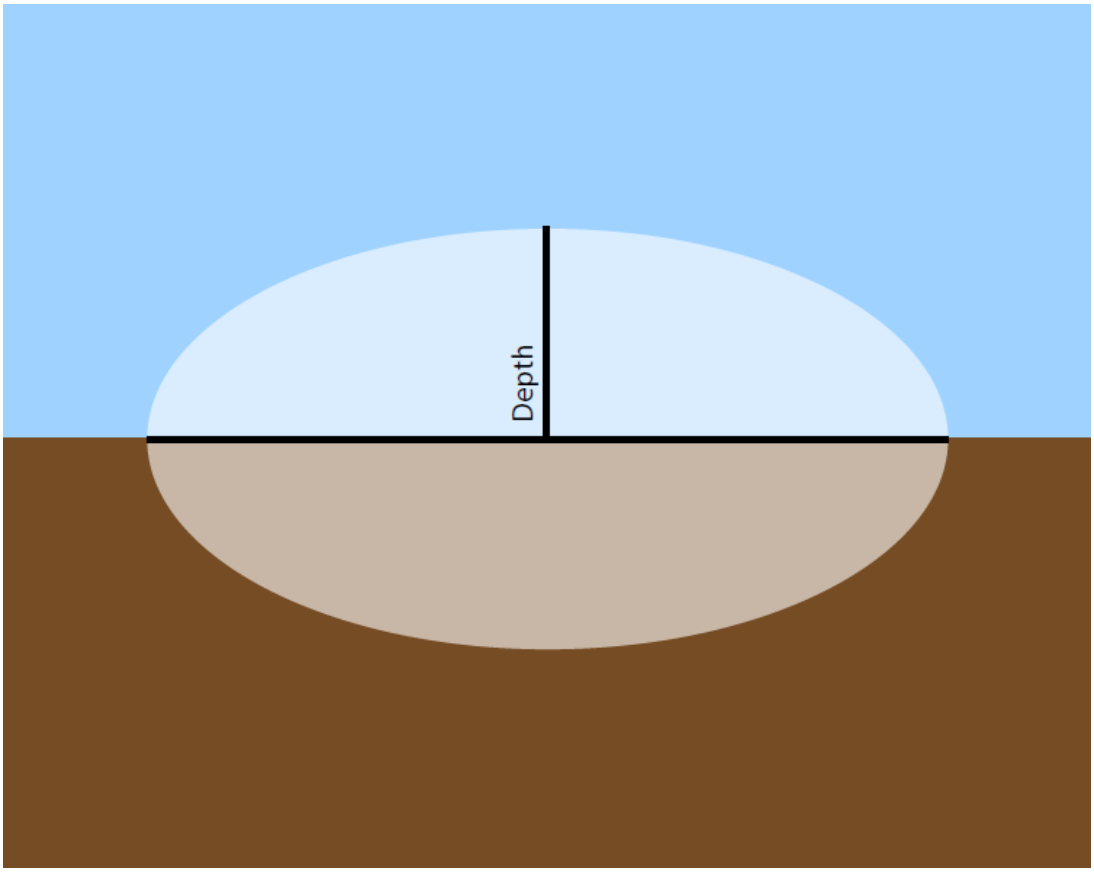

Figure 4. A cross-sectional view of modeling the snow pack as the top half (vertical semi-axis c, represented by the thickness) of an ellipsoid intersecting the plane of the landscape to form an elliptical base (semi-major and -minor axes a and b).

A linear regression was then performed to compare the relationship between area and volume in the single-point volume estimates and the grid volume calculations and these regressions were used to adjust the single-point value estimates.

To adjust the single point volume estimates to reflect the grid volume (GV) measurements, a power regression model was calculated using the grid area (GA) and grid volume (GV). This was derived from a log-log regression (*Equation 5*) using the grid-snowpack measurements. When the log-log regression (*Equation 5*) is solved, we are left with our power regression model (*Equation67*). The β constant is the slope of the simple linear fit regression from the grided snowpacks. The α constant is derived from the regression expressed in *Equation 7*. The power regression model (*Equation 6*) is how the volume will be calculated for future field sampling events.

$$Log(GV) = log\alpha + \beta log(GA) \qquad (5)$$

$$GV = \alpha(GA)^{\beta} \qquad (6)$$

$$Where\ \alpha = e(\overline{\ln(GV)}) - \beta(\overline{\ln(GA)}) \qquad (7)$$

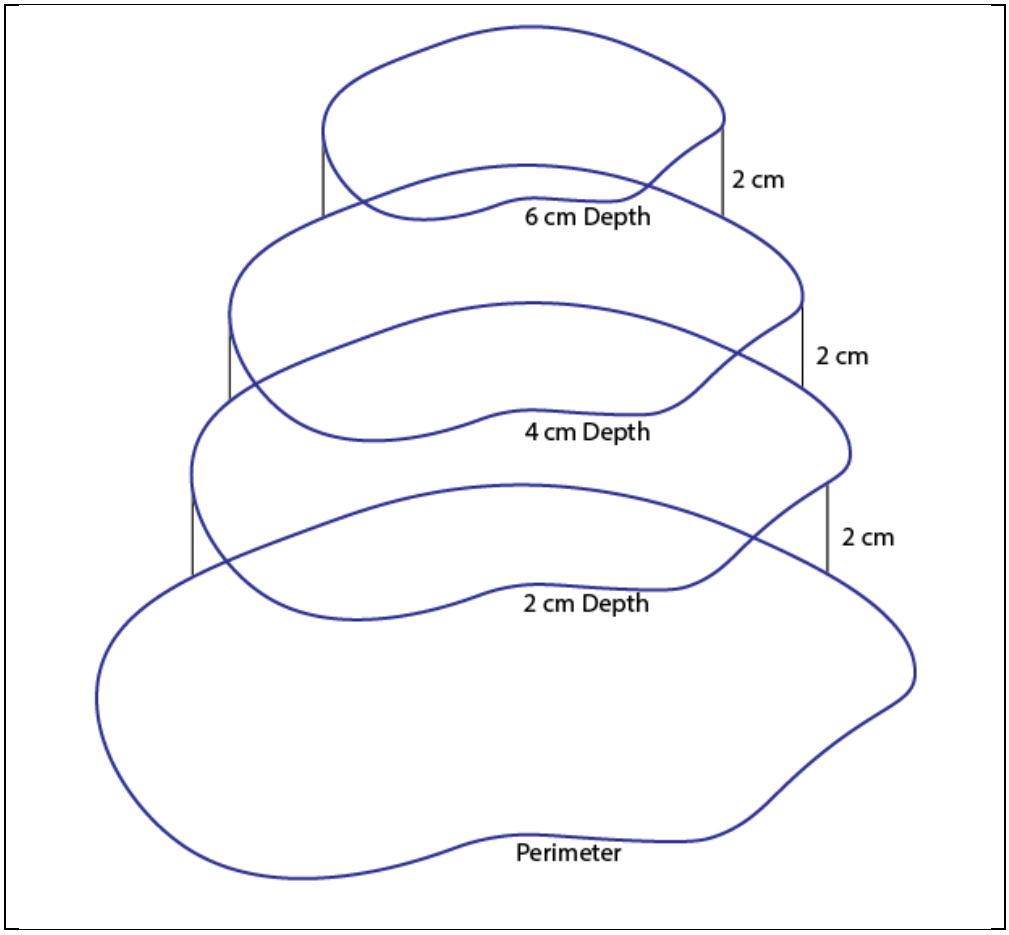

Figure 5. A schematic showing how each planar area layer was calculated, each contour was draw at a 2 cm scale. The cut and weigh method treats each contour line as a new area, with a height of 2 cm. When calculating the volume, 2 cm was used as the height between each planar layer.

3.5. Analyzing the Historic Record

To create a long-term record, a model was made using Python modules that consists of various Arcpy scripts. The Python model is necessary to process a dataset of this size, and it ensures consistency with future MCM LTER analyses of snow coverage. The model first uses the function "extract by mask" to crop the image to the five quadrats, significantly reducing the size of the images. If that quadrat is in a particular basin, it will go through another "extract by mask" execution, so only one quadrat is present. Once the images are cropped to their respective basin, the cropped image can be classified. The supervised classification scheme created was verified by the field sampling events, and by visually comparing the outputs to the input images. Training samples were added to the classification scheme until the desired results were achieved.

Shadows did affect the classification model, each image used was manually validated and removed outputs containing shadows and clouds. Once each raster cell is classified, the "cell statistics" function is executed. The cell statistics function expresses how many pixels are in each class- snow or barren ground. The cell statistics attribute table is exported and converted to an excel file. Each executed quadrat has its own excel sheet. The python model is posted on GitHub (https://github.com/KatieMcNultyMCMLTER/SnowClassificationMCMLTER) and below in Appendix A.

The excel sheets are then merged into one and the total areas and volumes can be calculated for each date. The spatiotemporal changes through time can be seen in this new long-term record. Due to the continuously changing landscape of the valley, the masked layer may need to be edited throughout the years; particularly at Lake Fryxell. A flow chart of the process is displayed in *Figure 6*. Quality control and data validation were performed in multiple steps, to ensure the outputs were reliable data. The cell statistic quadrat rasters were manually sorted through ArcGIS Pro, to ensure there were no clouds or partial coverage within the quadrat. The end members, outliers, and random samples were selected from the python-generated snow area outputs and manually validated. The end members were identified as the images with the most and least amount of snow area calculated within the normal range. The outliers were the snow area calculations outside of the normal range.

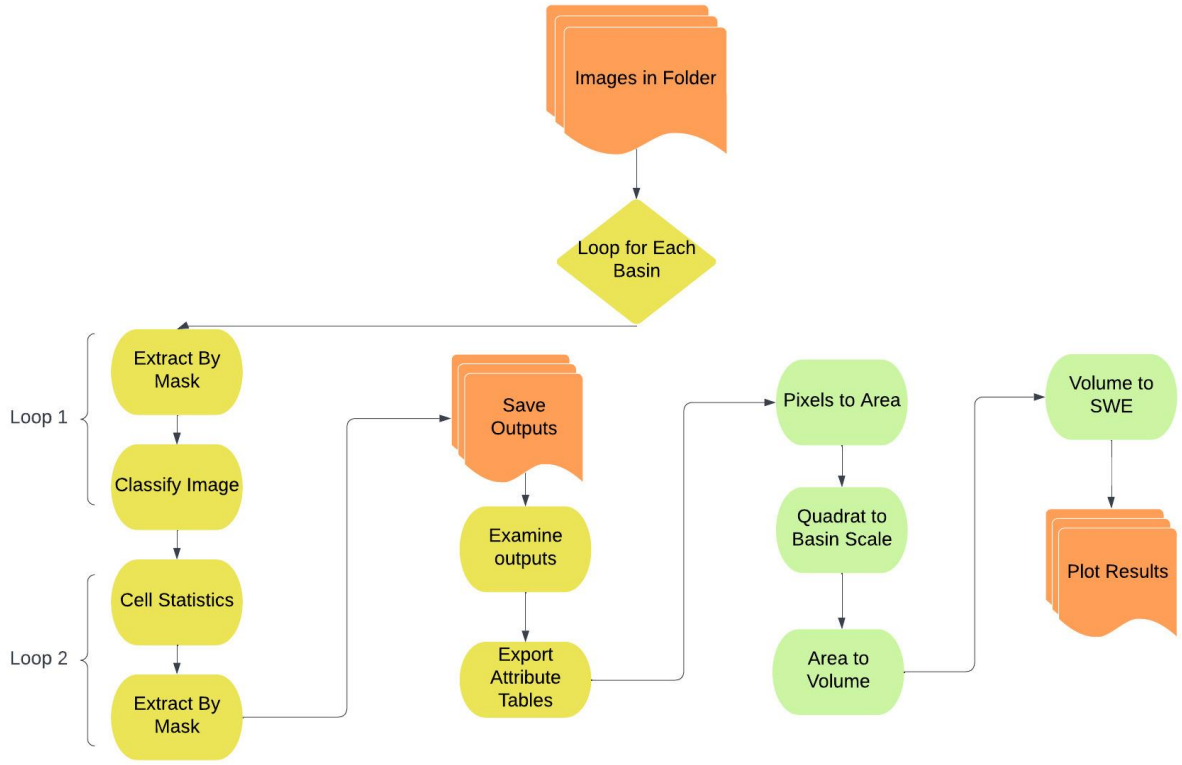

Figure 6. A flow chart of the model process. The orange indicates when new files are exported into folders. The yellow boxes indicate the use of the ArcGIS Pro python model for processing. The green indicates the calculated area, volume, and SWE relationships that are processed in Microsoft Excel.

3.6. Basin Calibration

To calibrate the ArcGIS Pro model to the field-collected data, a classification scheme was made with the panchromatic images that were collected during the time of snowpack sampling. The spacecraft targeting manifest is not public information, and so it was impossible to plan for field validation at the same time as satellite image collection. As a result, no images were collected on the same day as the sampling events. The Explorers Cove basin had images before and after the sampling event; both images produced the same SWE equivalent from the calculated areas. Fryxell had images within three days of sampling. Hoare had images within 7 days of the sampling event. Both East and West Lobe Bonney Basins had images within a day of sampling. The classification scheme was created so the image-derived quadrat snowpack areas equaled the field-calculated snowpack areas.

The supervised classification scheme uses the observed albedo to classify each pixel (Wang, 2015)(Appendix A). The classification scheme gives a Boolean value for each pixel in the image. A Boolean value has only two possible outcomes, true or false, or in this case, snow, or no snow on the valley floor. The classified image output will only have two classes, snow or

barren ground. When the calculated snow areas from the quadrat matched the field-measured values, the classification scheme could continue to be used for further analysis. Manual validation of other imagery and classified images was also performed to verify the accuracy of the classification scheme. Panchromatic images were used for this study because they are higher resolution and began collecting data in 2001, while the multispectral images are only present in the record beginning in 2009.

To extrapolate the amount of snow measured in each quadrat to reflect the total amount of snow within that basin, the basins had to be calibrated. For this calibration, only images that covered the entire basin were used. As previously stated, this type of coverage is rare in TV. When multiple images covered an area for one day, the images were mosaiced using the raster calculator. The raster calculator is a spatial analysis tool that uses a programmed algebraic syntax that uses the slope from each cell in a raster to match the cells in one raster with the corresponding cells in another raster file (Wang, 2015). The glaciers and ice-covered lakes were masked for this analysis. Masking these features is necessary because the albedo of these features will have the same spectral properties as the snow on the valley floor. This mask layer is included in the model package; however, the layer may require a manual update when necessary. For example, the lakes change shape as lake levels rise and fall; this is most notable at Lake Fryxell.

The full basin images were classified using the calibrated classification scheme and then the extract by mask tool was used to clip the classified image to the area of the quadrat (Wang, 2015). Both classified images were then run through the cell statistic tool in ArcGIS Pro; this tool counts the total number of cells in each classified section (snow or barren ground). The total amount of snow in the basin versus the total amount of snow in the quadrat was then compared. There is a seasonal component to the relationship between the amount of snow present in the basin versus the quadrat. Therefore, two basin-to-quadrat correlations were made based on early-season (October to December) and late-season (January to March) trends. The basin calibration makes it possible to estimate snow coverage over the entire basin by only measuring the amount of snow in the quadrat. The quadrat approach shortens processing times and makes it possible to derive basin-wide coverage estimates in scenes where parts of the basin are covered by clouds.

Chapter 4. Results

4.1 Satellite Coverage Analysis

While satellite imagery provides a long-term record, multiple steps were taken to eliminate as many data gaps as possible. When determining the locations of the 250 m x 250 m quadrats, a density map was created to determine where the most cloud-free images were collected (*Figure 7*), as described in Section 3.2. While the quadrats were in historically cloud-free areas, there were still some data gaps in the historic satellite imagery dataset. The variations in the orbital paths of the satellites, likely influence the amount of coverage at a given area. West Lobe Bonney and East Lobe Bonney basins had the least amount of data due to the frequency of coverage and cloud cover. Explorers Cove basin often did not have full basin satellite coverage and had the most images removed from the dataset due to cloud coverage. Imagery at the very beginning of the austral summer season, and during the late season was sparse due to increased cloud cover and lack of coverage.

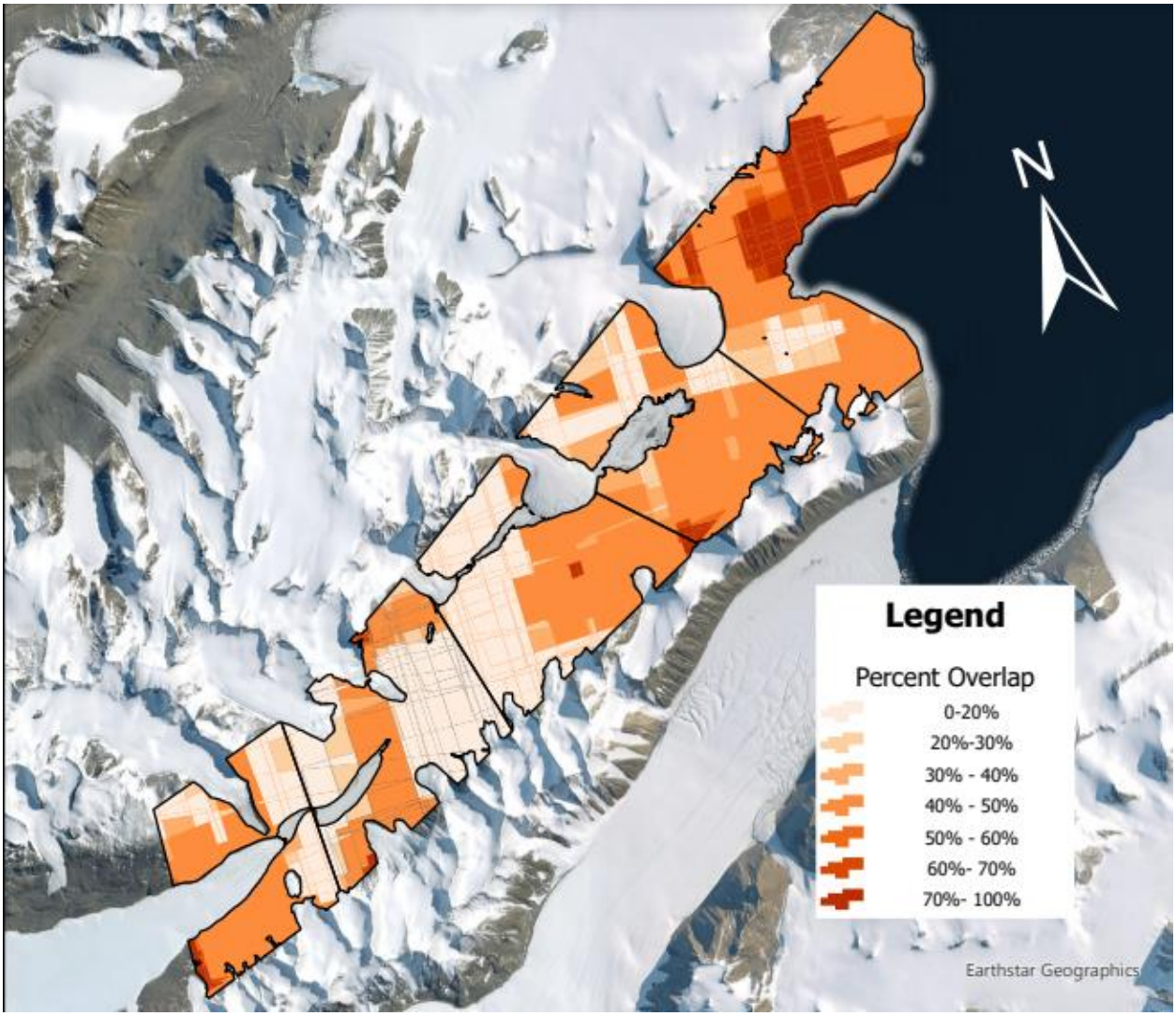

Figure 7. Frequency analysis of satellite coverage between 2001 and 2021. The darker areas represent the areas with the most cloud-free imagery coverage, and the lightest color represents the areas with the least cloud-free imagery coverage. The darker areas have a higher probability of containing the most usable images for this study.

4.2. Snow Volume Calculations

The grid snowpack contour maps show the deepest portion of a snowpack is not necessarily in the center (*Figure 8*). As observed in the field and by Eveland et al. (2013), microtopography on the valley bottom in TV influences snow accumulation and melt. This is most notable in the East and West Lobe Bonney snowpacks, where the deepest part of the snowpacks were located adjacent to the lee side of a microtopographic feature. While the complex geometries and thickness distribution of the snowpacks are dynamic, a strong area-volume logarithmic relationship was found (*Figure 9*).

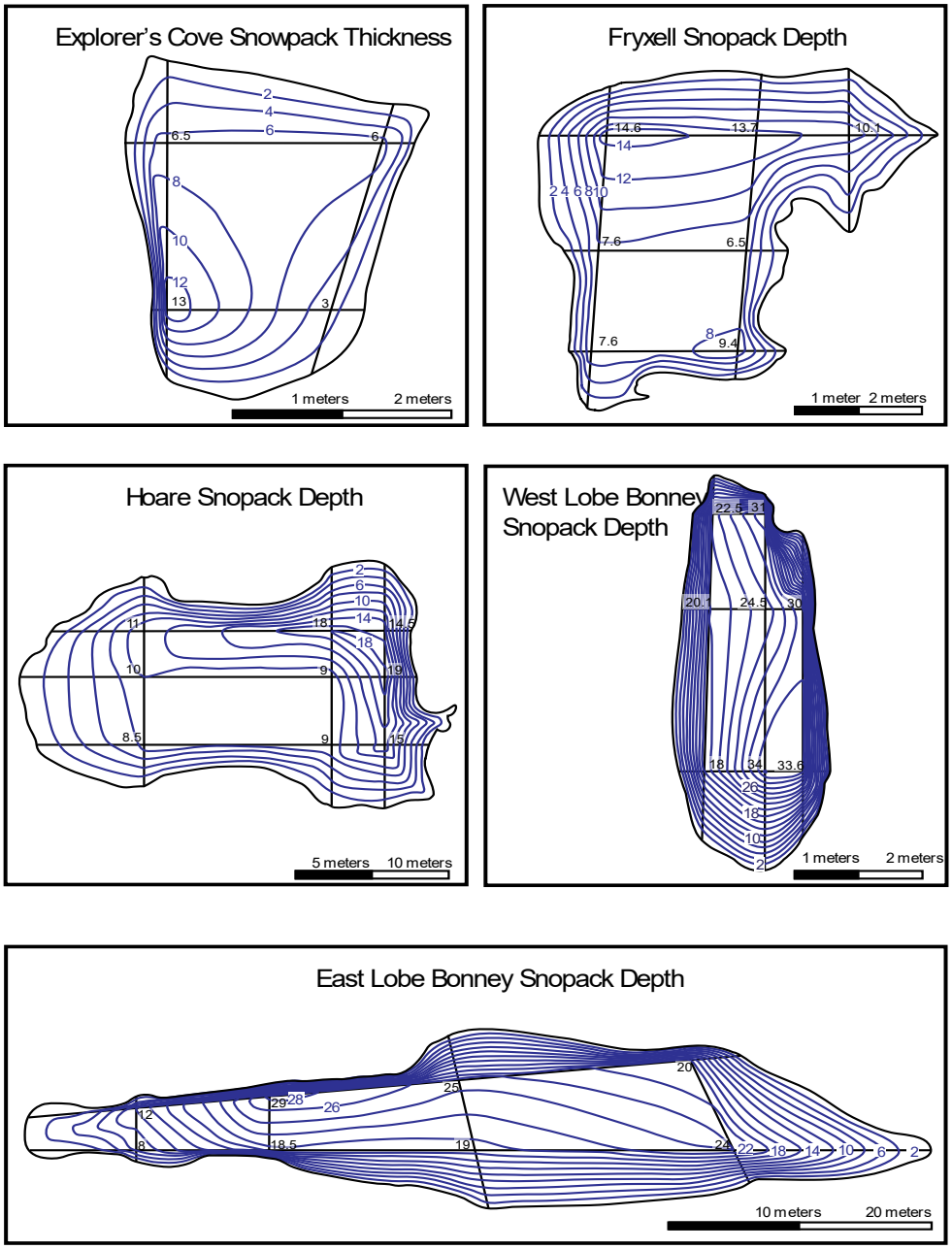

Figure 8. The grid-snowpack contour maps show the depth profile at 2 cm intervals (blue lines). The black numbers indicate the depths at each sampling profile. The black lines indicate the transects between each sampling point. The perimeter of the snowpack (black outline) was measured using GPS track data.

The snow densities measured in both the single point and grid measurements were homogenous over the sampling period. The average density of the snowpacks is 0.45 g cm^{-3}, which is defined as wet snow. This suggests the snow measured was deposited before the austral summer season, and the snowpacks already began compaction and metamorphosis before sampling occurred. Wet snow increases the cohesive resistance of the snowpacks, lowering the

probability snow will be remobilized (Li and Pomeroy, 1997). This also suggests summer snow deposition is insignificant in the hydrologic budget of the valley. While late season SWE measurements may not affect the hydrologic budget of the valley, the amount of albedo from late season snow is still important to monitor.

When comparing the calculated areas and volumes from the single point measurements (*Equations 2 and 3*) and the grid snowpack measurements (*Figure 9*), it is observed there is a strong area-volume relationship. While the single-point area volume relationship (*Figure 9*) shows a stronger linear relationship than the grid snowpacks (R^2= 0.988, P=0.367, Pearson's R= 0.994 vs. R^2= 0.942, P=0.182, Pearson's R= 0. 0.978), the grid snowpacks are more accurate due to the higher resolution (*Figure 8*). Therefore, the single-point volume estimates must be adjusted to reflect the grid-snowpack measurements.

The adjusted single point volume estimates reflect the grid volume measurements, a power regression model was calculated (*Equation 7*). The power regression model is what will be used for future single-point field measurements, and the grid linear relationship will be used to convert the historic image-derived area to volume because the grid-area calculation is the most like the image-calculated areas.

When the amount of debris in the snowpack was sampled, the mass of the solid debris was less than the detection threshold of the balance. If the snowpacks contained detectable levels of debris; the presence of debris can effect the spectral properties of the snowpack, thus influencing the classification model. The presence of debris can also add error to the SWE measurement; however, these separate SWE samples indicate there is no influence on these density measurements, so no further adjustments need to be made.

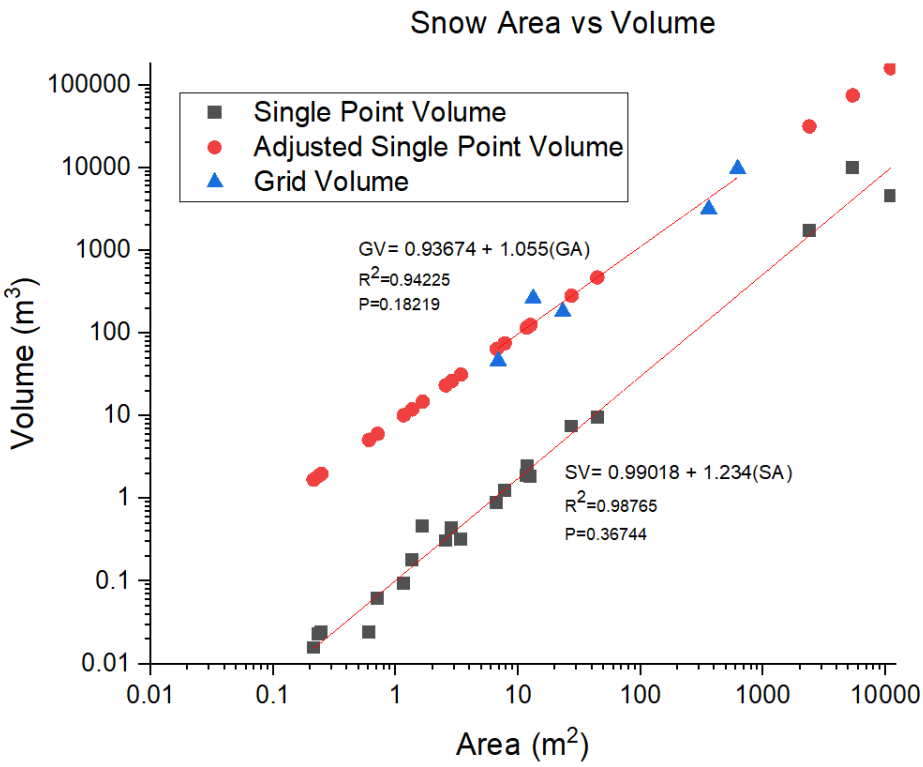

Figure 9. Adjusted area volume relationship between the grid snowpacks (blue triangle) (R^2= 0.942, P=0.182, Pearson's R= 0. 0.978), and the single-point snowpacks (grey squares) (R^2= 0.988, P=0.367, Pearson's R= 0.994). The red circles show the adjusted single point measurements using the calculated power function from Equation 7.

4.3. Basin Calculations

The calibration between the basin and the 250 m x 250 m quadrat was completed using historic satellite imagery as described in section 3.6 (*Figure 10*). Some full basin images were not included in the calibration due to cloud cover or shadows. The classification scheme can detect small snowpacks, as seen in *Figure 10b*, where the light snow accumulated in the ice-wedge polygon depressions is detected by the classification scheme.

While calculating the relationship between the total volume of snow in each basin versus the total snow in each quadrat, it was observed there is a seasonal component to the relationship. Due to this observation, the basin calibrations are separated into early season and late season relationships (*Figures 11 and 12*). The early season is defined as September through December and the late season is defined as January through March. The late season calculations were more variable and unreliable. The early season relationship for all basins has an R^2 of 0.952 P<0.01(*Figure 11f*). The late season relationship for all basins has an R^2 of 0.127 P<0.01(*Figure 11k*). All early season basin to quadrat calculations have strong relationships, except for West Lobe Bonney, which has a low R^2 of 0.178, P<0.01 (*Figure 11e).*

4.4. SWE Budgets through time

From 2004 to 2022, the average early season snow area is 65.26 km^2, the average snow volume is 0.0688 km^3 (SWE of 0.0310 $km^{3)}$, and the average SWE depth is 75.72 mm. In the Explorers Cove basin historical record, 2009 has the highest snow area and SWE *(Figures 13 and 14*). In Fryxell basin, the years with the highest snow area and SWE were 2013 and 2016. In Hoare basin, the years with the highest snow area and SWE were 2016 and 2018. In East Lobe Bonney, the years with the highest SWE were 2017 and 2020. In West Lobe Bonney basin, the years with the highest SWE were 2017, 2019, and 2020. West Lobe Bonney and East Lobe Bonney basins showed a slight increase in the amount of snow coverage over the years 2004 through 2022 (*Figure 13, Figure 14, Figure B.2-10*). West Lobe Bonney basin specifically saw an increase starting in 2017. On average, Explorers Cove has the highest amount of snow coverage, and the amount of snow coverage in TV decreases in the west direction (*Figures 13, 14, and 15*). While Explorers Cove has the largest range of data, there are no outliers (*Figure 15*). In West Lobe Bonney, from 2017 on, there has been an uncharacteristically high increase in the total area of snow coverage (*Figures 13, 14, and 15*).

All basins show a decreasing trend from September to December, except for Explorers Cove basin, which has a slight increase from September to October (*Tables 2 and 3, Figure B.2-10*). In the historical dataset, the month of September had few images compared to other months in Explorers Cove basin; which may be due to satellite coverage properties or environmental factors, such as clouds. The Explorers Cove basin also shows a slight decrease in snow area coverage in the record (*Figures 13 and 14*).

From September to December the amount of snow coverage in all of TV decreased by 65% (not including the September estimates from West Lobe Bonney), in Explorers Cove, the amount decreased by 56%, in Fryxell basin the amount decreased by 75%, in Hoare basin the amount decreased by 77%, in East Lobe Bonney the amount decreased by 63%, and in West Lobe Bonney the amount from October to December decreased by 65% (*Table 2*).

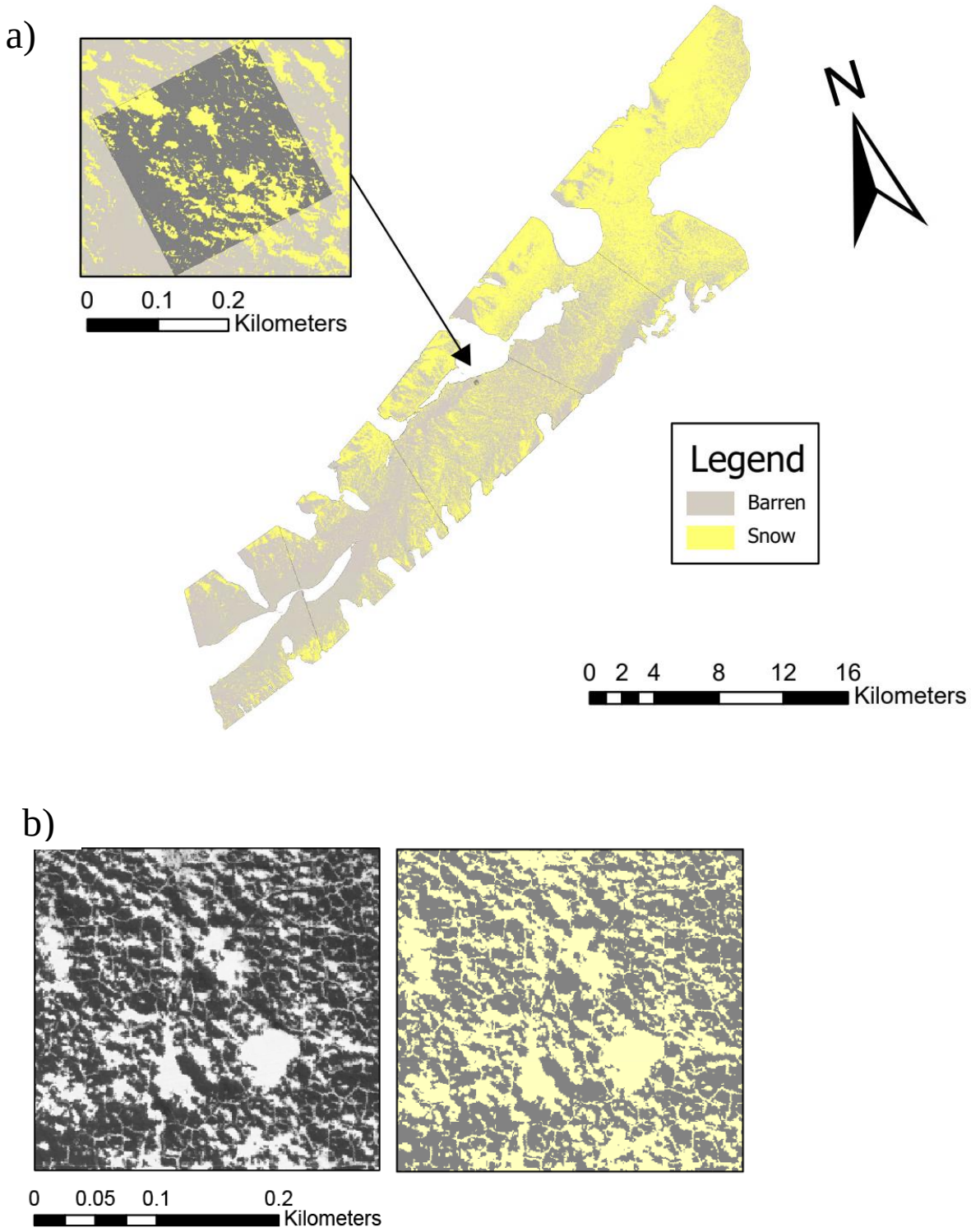

Figure 10. a) An example of the classified images, where grey represents the bare ground and yellow represents snow coverage. The Hoare Basin 250 m x 250 m quadrat is displayed in the call out box. The images used for this classification were acquired on November 17, 2009. b) A side-by-side comparison of a panchromatic image and classified image.

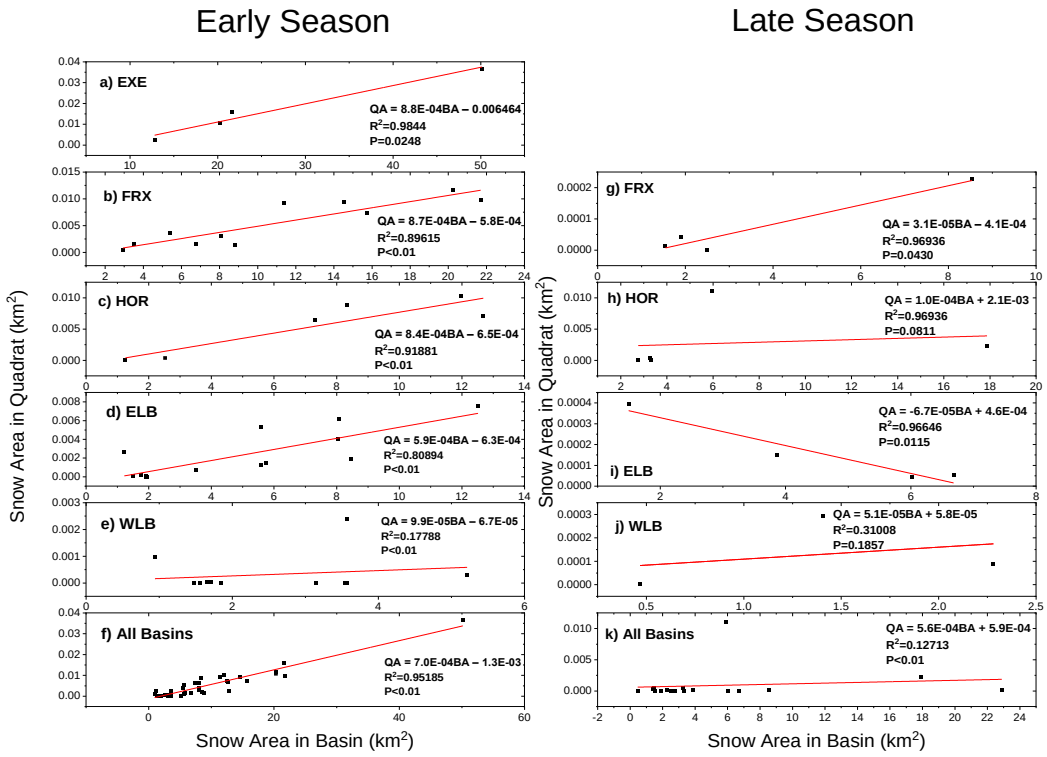

Figure 11. Plots showing the relationship between the snow area in each basin versus the snow area in each quadrat in the early season and late season. The red lines are best fit.

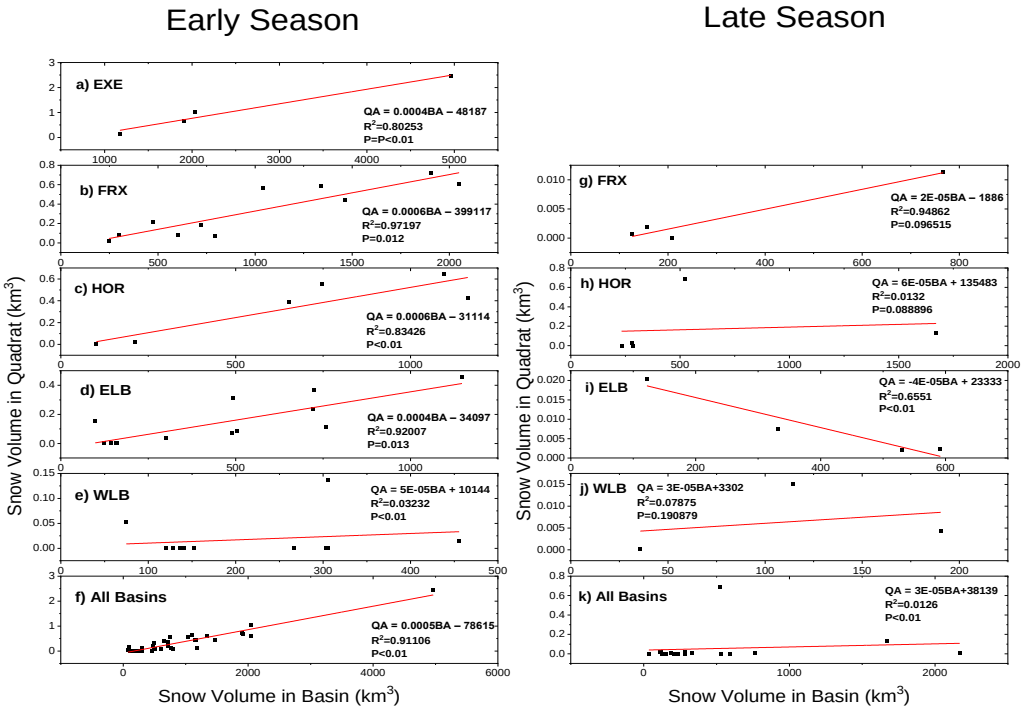

Figure 12. Plots showing the relationship between the snow volume in each basin versus the snow area in each quadrat in the early season and late season. The red lines are best fit.

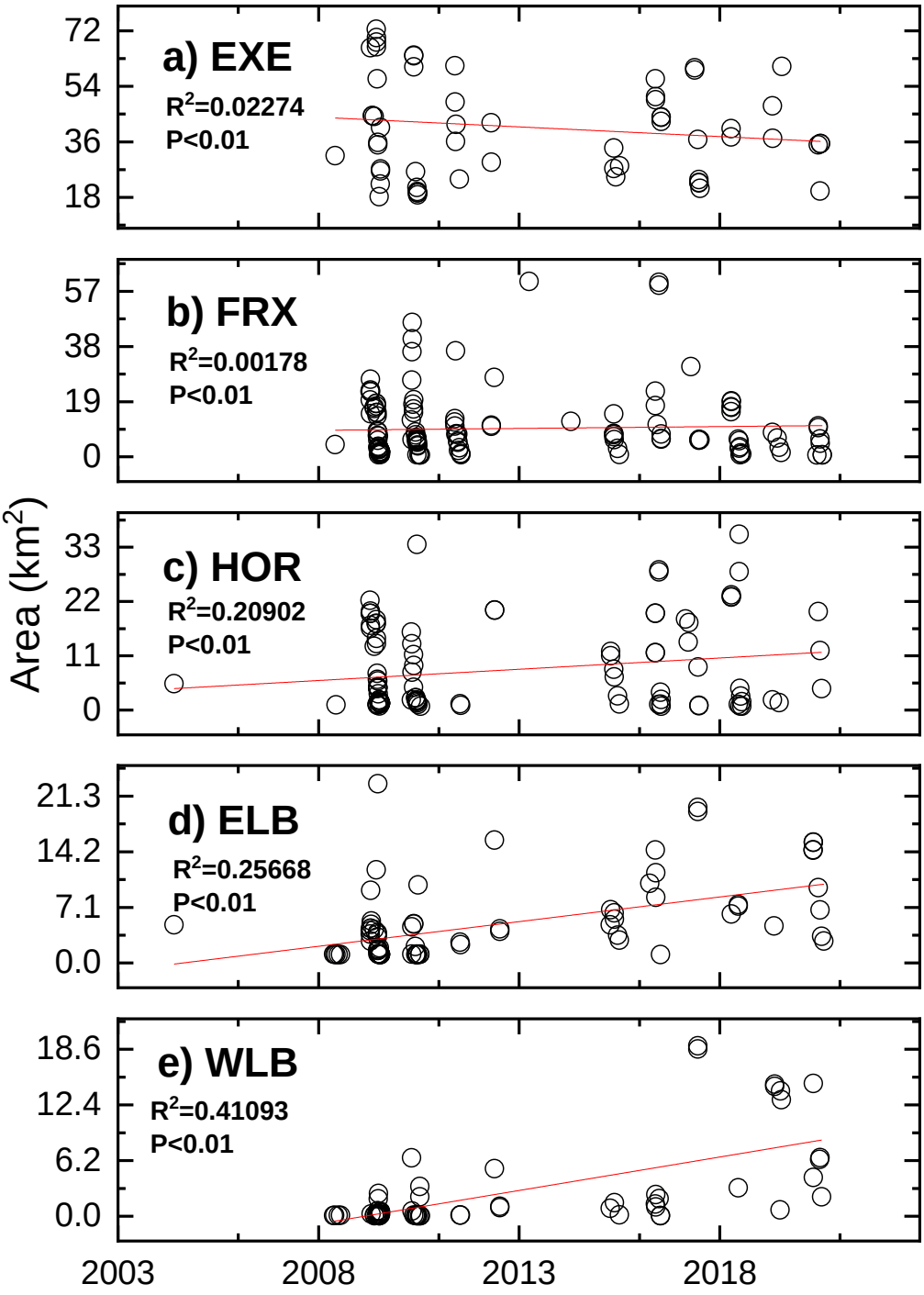

Figure 13. Historic early season snow area (km^2) coverage in each basin from 2004 to 2022.

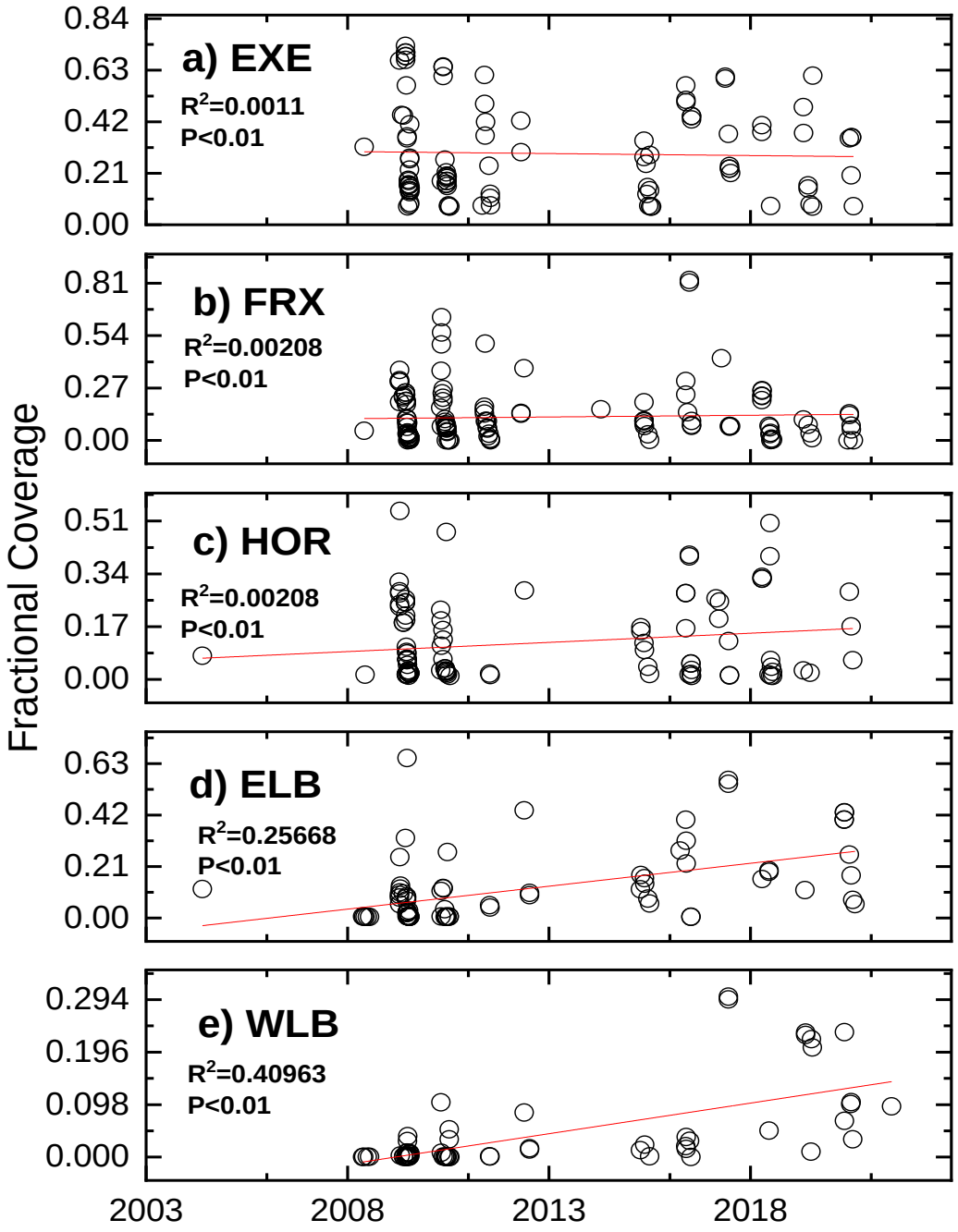

Figure 14: Historic early season fractional snow coverage versus barren ground in each basin from 2004 to 2022.

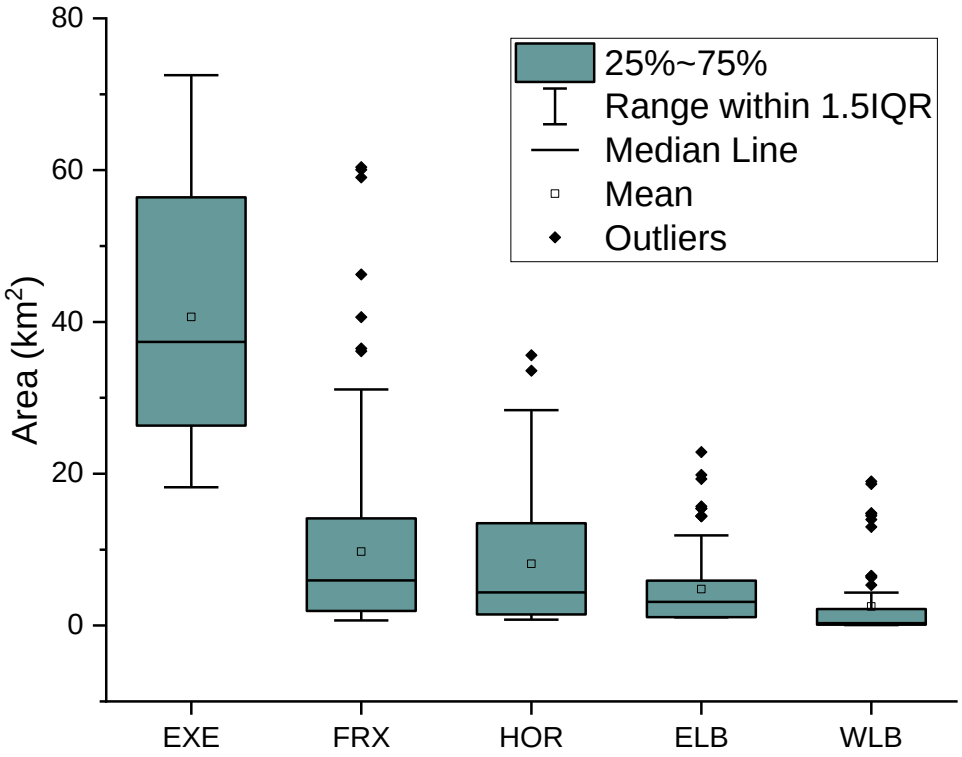

Figure 15. Shows the range of snow coverage area during the early season from 2004 to 2022 in each respective basin. The boxes represent the range of areas between the 25th and 75th percentile. The horizontal black line inside the box represents the median value in the dataset. The small black square represents the mean value in the dataset. To find outliers, the interquartile range (IQR) for the data is multiply the constant 1.5; this is displayed with the I shaped bar; all outliers are identified by a black diamond. Explorers Cove has the highest range of snow coverage, and highest range realitive to the mean.

Table 2.. Monthly early season average snow area in TV and sub-basins. *WLB does not have an average for the month of September, because there was only one measurement* available.

Month	**EXM (km^2)**	**FRX (km^2)**	**HOR (km^2)**	**ELB (km^2)**	**WLB (km^2)**	**All of TV (km^2)**
September	43.17	33.10	20.33	8.81	NA	105.41
October	43.74	27.13	10.53	11.54	5.24	98.17
November	35.63	14.89	8.59	8.81	2.60	70.52
December	18.92	8.02	4.52	3.24	1.81	36.52

Table 3. Monthly early season average SWE depth in TV and sub-basins. *WLB does not have an average for the month of September, because there was only one measurement available.*

Month	EXM (mm)	FRX (mm)	HOR (mm)	ELB (mm)	WLB (mm)	All of TV (mm)
September	206.21	235.21	136.50	67.39	NA	381.26
October	208.93	192.79	70.70	88.27	56.86	177.54
November	170.19	105.81	57.68	67.39	28.21	69.56
December	90.37	56.99	30.35	24.78	19.64	18.87

The average early season snow coverage by area, volume, SWE, and SWE depth are shown in *Table 4*. The average late season snow coverage by area, volume, and SWE are shown in *Table 5*. The early season estimates show a decreasing trend in the amount of snow area coverage from the coast westward (*Table 4*). The average early season area coverage by snow in TV from 2004 until 2022 is 65.26 km^2 (*Table 4*) which is an average of 14% of the ground covered by snow. On average, during the early season, the percent of ground covered in snow in Explorers Cove is 41%, in Fryxell it is 15%, in Hoare it is 11%, in East Lobe Bonney it is 8%, and in West Lobe Bonney it is less than 1%. The average early season snow area volume in TV from 2004 until 2022 is 0.0688 km^3. The average early season SWE in TV from 2004 until 2022 is 0.0310 km^3. The average SWE depth in TV from 2004 to 2022 is 75.72 mm.

In the early season, the average amount of snow coverage in Explorers Cove is almost three times higher than the amount of snow coverage in Fryxell Basin (*Table 4*). There is only a slight increase in snow coverage from Fryxell to Hoare basin (T*able 4*). From the Hoare basin to the East Lobe Bonney basin the amount of snow coverage is approximately halved, and from East Lobe Bonney to West Lobe Bonney the amount of coverage is halved again (*Table 4*). The amount of snow coverage in Explorers Cove basin is approximately 90% higher than the amount of snow coverage in the West Lobe Bonney basin (*Table 4*).

The total average early season snow coverage in all basins (*Table 4*) is just over half the average September snow coverage (*Table 2*). The West Lobe Bonney Basin does not have a September average due to lack of coverage; however, the October average is more than double the early season average for the basin.

In East Lobe Bonney basin, the late season estimates of snow area coverage (*Table 5*) are larger than the early season estimates; this is not consistent with field observations and observations from historic satellite imagery. However, the late season dataset for East Lobe Bonney is smaller than the early season dataset. The East Lobe Bonney late season available images are mostly comprised of more recent imagery; whereas the early season dataset encompasses the entire span of the record. So, the late season East Lobe Bonney record is reflecting the recent increase in snow area coverage in both West and East Lobe Bonney Basins (*Figures 13 and 14*). This increase post-dates previous snow studies in TV and should be continually monitored by the MCM LTER using this snow model. The Explorers Cove basin late season estimate was calculated using the early season calibration, because there were not enough full-basin images to create a late season calibration (*Table 5*).

Table 4. Early season averages from 2004 to 2022.

Basin	Early Season Snow Area Average (km^2)	Early Season Snow Volume Average (km^3)	Early Season SWE Average (km^3)	Depth of SWE (mm)
EXM	40.75	0.0430	0.0193	194.64
FRX	9.58	0.0101	0.0045	68.06
HOR	7.44	0.0079	0.0035	49.97
ELB	4.79	0.0051	0.0023	36.65
WLB	2.70	0.0028	0.0013	29.29
All of TV	65.26	0.0688	0.0310	75.72

Table 5. Late season averages from 2004 to 2022.

Basin	Late Season Snow Area Average (km^2)	Late Season Snow Volume Average (km^3)	Late Season SWE Average (km^3)	Depth of SWE (mm)
EXM	5.06	0.0053	0.0024	24.17
FRX	6.92	0.0073	0.0033	49.17
HOR	4.15	0.0044	0.0020	27.86
ELB	6.35	0.0067	0.0030	48.57
WLB	1.02E-03	1.1E-06	4.8E-07	0.01
All of TV	22.49	0.024	0.011	31.12

Chapter 5. Discussion

This study was able to make observations on the spatiotemporal changes of snow coverage in TV over an 18-year period, from 2004 until 2022, using satellite imagery. The data extracted from the satellite imagery were used to estimate both the areal coverage and SWE of snow in TV. While high-resolution satellite imagery is an effective tool for investigating spatial data, some limitations remain. One limitation is that satellites can rarely collect images spanning the entire extent of TV in one day, at the high resolutions required for this investigation. Another major limitation is the presence of clouds in the images that may block or obscure the ground below. To address these limitations, the quadrats decreased the sampling size and increased the probability of usable imagery data. The division of TV into five sub-basins was also beneficial to reflect each basin's hydrologic controls. There were noticeable variations between the three eastern basins- Explorers Cove, Fryxell, and Hoare, and the western basins- East and West Lobe Bonney, and within the five basins the amount of normal snow coverage unique. Another limitation of using satellite imagery is the earliest data is from 2004, whereas the meteorology stations were established prior to the MCM LTER inception in 1992. To further address these data gaps, future work can be completed to make the connections between the AWS data and the satellite data. While there were some limitations and data gaps in this record, a successful baseline dataset was created and a very strong relationship between the area and volume of the snowpacks in TV was determined.

5.1 Ground Truth Area vs Volume Work

There is a strong relationship between the area and volume of snowpacks in TV which provides the opportunity to predict the volume of snow on the ground from areal measurements from space. The snowpacks sampled in the field varied in scale, from submeter snowpacks to 10,000 m^2 snowpacks, so there should be no size bias skewing the area-volume relationship up to the maximum size that was measured. Both the methods of single-point and grid sampling were effective in calculating volume, as shown in *Figure 9*. However, this study was only able to measure snowpacks on the ground below 10,000 m^2 in area and so there is no indication of how the relationship holds at larger scales. It is anticipated that the shape of large areas of snow does not continue to thicken towards the center, so the volume estimates in this study are likely overestimates. The model will underestimate the total amount of snow area when the snow area on the ground is smaller than the resolution of the satellites.

The detailed grided volume measurements showed that the deepest part of the snowpacks is not necessarily in the center of each snowpack, however, the volume can still be measured regardless of the size of the snowpack. Like Eveland et al. (2013), this research found microtopographic features influence areas of snow accumulation. By successfully creating a model that relates snow area to snow volume, SWE measurements on basin-wide scales can be gathered with accuracy. Microtopographic features may be just as important in snow coverage as precipitation source. While the Explorers Cove basin is closest to the source of precipitation, it also has many more microtopographic features, where snow can accumulate, as compared to West Lobe Bonney basin, which has steep valley walls and fewer microtopographic features for snow to accumulate. The microtopographic features can shield previously precipitated snow from erosion, and collect snow blown from higher elevation areas.

It should also be noted that all the snowpacks during sampling had a homogenous density (0.45g cm^{-3}), which is classified as wet snow. Wet snow indicates the snow has already begun

the process of compaction and or melting. The absence of fresh snow in the snowpacks during the summer season sampling suggests most snow is likely to accumulate in the winter season. This also indicates much of the early season summer snowpacks will likely not redistribute with winds because the snow is too dense and compacted. This would mean that fresh snow in the summer season is likely a result of precipitation events or blown in from the ice shelf or ice sheet; an established snowpack present at the beginning of the summer season is more likely to ablate (sublimate or melt) than be fully redistributed by wind. The properties of wet snow will also affect the energy budget differently than fresh snow.

5.2 TV Coverage Through Time

This is the first estimate of valley-wide snow coverage and SWE through time using satellite imagery. By using both the image classification model and the area-volume model, the early season estimates of snow area and SWE can be determined for the five basins in TV. The basin-to-quadrat relationships relates the 250 m x 250 m quadrats to basin-wide scales, so total volume and SWE can be calculated by only analyzing a small area of the basin.

Each sub-basin has a unique micro-climate and hydrologic influences, so the individual basin estimates are a better representation of snow coverage trends through time. In the basin data, Explorers Cove, Fryxell, and Hoare do not show a significant change in the total snow coverage.

While there is an increase in the East and West Lobe Boney basins, the amount of total snow coverage is still much smaller than the total amount of snow in the eastern basins. In Explorers Cove and Fryxell, the percentage of snow covering the valley floor is often above 50% in the early season. Over 50% snow coverage is important because snow coverage provides a proxy for valley-wide albedo. Albedo measurements can lead to more precise energy balances in the future; especially when paired with AWS data. The albedo from snow coverage blocks solar radiation from being absorbed into the valley floor and the total energy balance controls the amount of melt generated each season (Bergstrom et al., 2020; Dana et al., 1998; Fountain et al., 1999). Snow coverage limiting the amount of solar radiation being absorbed results in less energy available for the primary producers in the soil; this may indicate less productivity in Explorers Cove and Fryxell.

In all five basins, the abundance of snow during each season, decreases monthly as the season progresses. This steep decrease is likely due to much of the snow being deposited in the winter months. The austral summer brings increased solar input and degree days above freezing with little precipitation input, resulting in a net loss of snow coverage by ablation.

The total accumulated SWE depth in TV is 75.72 mm (*Table 4*) is slightly higher than the total SWE precipitation estimates of Myers et al. (2022) of 1 to 58 mm (yearly received precipitation from August to May), and lower than the Fountain et al. (1999) estimates 100 mm SWE of precipitation per year. The 1 to 58 mm SWE estimates from Myers et al. (2022) represent the amount of yearly precipitation received at the AWS. Our estimates reflect total SWE accumulation in TV at the beginning of the austral summer season. The discrepancy could be caused by 1) there is a large amount of snow deposition during the austral winter, that cannot be detected by the AWSs and 2) without an added spatial component, the AWS greatly underestimate the amount of snow present in TV, or 3) a large component of snow on the ground is wind-blown. The latter is the most likely of these in combination with the SWE values from this study likely being overestimates as discussed above. The difference between yearly (August through May) estimates from the AWS and the total SWE at the beginning of each summer

season could indicate some snowpacks can persist for multiple seasons; so although the precipitation wasn't measured by the AWS for that season it is present in TV. The SWE and SWE depth tells us how much potential surface water is available for that coming season. The abundance of surface water contributes to productivity in the valley, velocity and persistence of the streams (but most comes from glacial melt), and connectivity between the basins.

The late season data is too sparse to be reliable and should not be used as a baseline data set; these data only show a rough estimate of the general trends for late season snow accumulation in TV. The late season is unreliable because 1) there is less usable imagery to make quadrat to basin calibrations, and 2) many factors contribute to snowpack persistence, such as degree days above freezing, solar radiation, and soil temperature. If the frequency of imagery acquisition was increased in the late season, there would be more usable data to create calibrations. This study suggests most of the snow accumulation in TV occurs during the austral winter, where there is little to no solar input. Solar input is the main driver of energy balance in TV and is difficult to capture on a large scale (Bergstrom et al., 2020).

The Fryxell, Hoare, and East Lobe Bonney Basins all have slightly negative late season basin to quadrat relationships; meaning the model will calculate the fractional abundance to be lower in the whole basin than the fractional abundance of snow in the quadrat. This result is not likely and may indicate there is some control allowing snow to persist in the quadrat area during the late season.

5.3 Spatial Variability

This study found that the most snow accumulation occurs in Explorers Cove and decreases westward, which agrees with Fountain et al. (2010), Myers et al. (2022), and Obryk et al. (2020). Explorers Cove has approximately 90% more early season snow coverage than compared to West Lobe Bonney; demonstrating most snow accumulation in TV is derived from the Ross Sea. The increased precipitation at Explorers Cove is due to moisture availability, and air mass dynamics (Fountain et al., 2010; Fountain et al., 2016; Kimura, 2007; Patterson et al., 2005). The moisture from the Ross Sea creates snow, but as the air mass moves westward, the snow drops; meaning the air mass becomes drier the more inland it progresses. As sea ice and the Ross Ice Shelf decrease, there may be more moisture availability for precipitation under certain SAM conditions (Patterson et al., 2005). The data from this research do not show an increase in snow accumulation through time in the Explorers Cove Basin, but we hypothesize as there is more open ocean resulting from climate warming, TV will receive more precipitation (Patterson et al., 2005; Vignon et al., 2021).

There is a subtle increase in average snow area coverage and SWE in Explorers Cove from September to October. This could be due to 1) fewer available images in September than in October, or 2) the monthly changes in the Amundsen Sea Low (ASL). From September to October the meridional winds move north and inland towards the MDVs, and the zonal ice drift moves further seaward (*Figure B.11*) (Kwok et al., 2017). The increase in the open ocean and winds can create more precipitation in TV (Patterson et al., 2005). After October the meridional winds and zonal ice drift remain do not significantly shift again during the summer season (*Figure B.11*) (Kwok et al., 2017), but the amount of monthly snow coverage in Explorers Cove basin decreases for the remainder of the season. This could indicate that ablation caused by solar input and degree days above freezing outweighs any additional precipitation inputs from the open ocean and prevailing winds. Another indication the October precipitation input in Explorers Cove Basin is relatively small compared to the winter inputs is, the October snow coverage

increase is not seen in Fryxell basin; the precipitation created during this October is not enough to accumulate westward.

While the Explorers Cove basin did show an increase in the October record compared to the other months, when all data points are analyzed (*Figure 13*), there was no change in average snow coverage over time. However, in East and West Lobe Bonney basins, there is higher snow accumulation throughout the historical record. Unlike Explorers Cove, the increased average snow cover in West Lobe Bonney does not necessarily indicate there is a nearby moisture source. This increase in snow coverage in the western basins is likely due to the amount of snow blown into the valley from the ice sheet during the winter foehn events (Fountain et al., 2010; Fountain et al., 2016). The air masses moving eastward are likely still dry, and the snow deposited is a result of foehn winds transporting snow eastward from Taylor Glacier (Fountain et al., 2010; Fountain et al., 2016).

As previously observed, the Nussbaum Riegel appears to act as a precipitation shadow to both the westward winds carrying snow from the Ross Sea and ice shelf, limiting snow into East Lobe Bonney Basin; and to the eastward winds carrying snow from the ice sheet, limiting snow into Hoare Basin, which supports results from other research performed by Fountain et al. (2010; 2016). Snow accumulation at the terminus of glaciers is known to increase the amount of spring melt (Fountain et al., 1998; Fountain et al., 1999). If West Lobe Bonney continues to have an increase in snow accumulation, this could result in higher liquid water inputs in the West and East Lobe Bonney basin soils at the beginning of each season.

5.4 Late Season Variability

This method is useful for estimating early season snow coverage, volume, and SWE. Late season estimates of total snow coverage were unreliable, due to the numerous factors that influence snow persistence, including total snow coverage, solar input, degree days above freezing, soil temperature, relative humidity, and wind. The amount of debris in the snowpacks was insignificant, so aeolian sediment likely does not influence late season variability; which is curious because aeolian sediment creates extreme differential melting on the lakes (personal observations).

When there are higher amounts of snow coverage, snow persistence will be longer due to the decrease of long-wave radiation absorption into the soils and emission back into the atmosphere. The amount of solar radiation input will also affect snow persistence, while cloud coverage creates data gaps in satellite imagery, the clouds increase albedo, reflecting and absorbing incoming shortwave radiation. Less solar input will result in longer snow persistence and more solar input will result in shorter snow persistence.

Degree days above freezing will influence snow persistence in the basins because it will impact the ablation of snowpacks. From 1997 to 2017, the average degree days above freezing at Explorers Cove is 13.1; from 1987 to 2017, the average degree days above freezing at Fryxell is 20.9; from 1985 to 2018, the average degree days above freezing at Hoare is 24.6; from 1993 to 2017, the average degree days above freezing at Bonney is 44.2 (Obryk et al., 2020). Of all the basins in the valley, West Lobe Bonney basin has the highest late season variability (*Figure 11*) and the highest number of degree days above freezing.

The soil temperature can affect snow persistence, because warming soils can melt snowpacks from the bottom up. The soil temperature, like snowpack persistence is controlled by solar input and degree days above freezing. Similarly, soil moisture can affect late season snowpack dynamics because with a wetter darker valley floor, more infrared radiation will be

absorbed and heat snowpacks from the bottom up. The relative humidity also affects snowpack persistence because drier air masses result in more sublimation and moister air masses result in more melting of snowpacks (Heymsfield et al., 2021). The wind can redistribute and erode snowpacks, but because most snowpacks in the summer season are wet snow, they are likely too dense to be redistributed; however late season winds can erode snowpacks. While all these factors that influence late season variability are monitored at the MCM LTER AWS, the data are spatially limited. With a higher frequency of satellite coverage, a connection between the AWS and satellite imagery can be made to determine snowpack controls and responses.

Chapter 6. Conclusions

This study was able to build a baseline dataset for early-season (September through December) spatial snow coverage and SWE in TV from 2004 until 2022. The image classification model created is an automated process to accurately measure basin-specific and valley-wide snow area. The snow area is the main factor in determining the albedo of TV. The albedo is the main driver for the energy balance of the valley (Bergstrom et al., 2020). The area volume model can accurately estimate SWE from the snow area estimates from the image classification model. The SWE is extremely difficult to measure on a large scale and field measurements and AWS does not account for snow already accumulated on the ground. The continued utilization of satellite imagery is important in remote locations like TV because collecting field data is often limited due to the amount of time and resources required to sample on the continent.

The long-term snow record created in the project can be used in comparison with other MCM LTER long-term records. With the use of this new dataset, a better understanding of forcings and feedbacks in TV can be determined. Some relationships to be further examined with this dataset are: snow cover and its impacts on soil moisture, soil temperature, permafrost depth, etc. While the cell statistic output and spot checks will be required manually in the future, this automated model ensures consistent and accurate snow estimates in TV.

Future work may also be completed to examine late season variability and snow persistence patterns. While many data gaps were eliminated by the basin-to-quadrat relationship, image availability, and cloud cover still limited the output dataset. If satellite coverage increases in frequency and extent in TV, a higher resolution dataset can be continued in the future, furthering a better understanding of these complex patterns.

To better understand the controls of snow in TV, a relationship between the snow coverage data, the AWS data, and regional indices such as SAM should be created to fill in satellite coverage data gaps. In the face of an anthropogenically induced warming climate, it is impossible to predict the future without a frame of reference. This study was able to build the baseline dataset needed to make future predictions about snow coverage dynamics in TV.

Appendix A. Python Program for Calculating Snow Area from Satellite Images

Below is the Idle and Jupiter Notebook code written for the Image classification model.

```
#Image Snow Classification Model
#Author: Katie McNulty

#update file pathways in the Define Variables and Set up Rasters
for Loops

####Before putting  images in the folder use the following two
scripts to rename and sort new images,
the images imported from the PGC must be edited before putting
them through the loops


#_____________________________________________________________________

##Move Files

import os
import shutil

srcpath = "File_Path_of_Images_To_Be_Imported"
srcfiles = os.listdir(srcpath)

destpath = "File_Path_Outputs"

# extract the three letters from filenames (Satellite Name)
destdirs = list(set([filename[0:4] for filename in srcfiles]))


def create(dirname, destpath):
    full_path = os.path.join(destpath, dirname)
    os.mkdir(full_path)
    return full_path

def move(filename, dirpath):
    shutil.move(os.path.join(srcpath, filename)
                ,dirpath)

# create destination directories and store their names along
with full paths
targets = [(folder, create(folder, destpath)) for folder in
destdirs]
```

```
for dirname, full_path in targets:
    for filename in srcfiles:
        if dirname == filename[0:4]:
            move(filename, full_path)

#_____________________________________________________________________

#_____________________________________________________________________

##Rename

import os

path = 'File_Path_of_Images_To_Be_Imported'
os.chdir(path)
os.listdir("File_Path_Saved")

for filename in os.listdir(path):
    oldname, file_extension = os.path.splitext(filename)
    #Only change [5:9] to extract new portion of file name
    newname = os.path.join(path, filename[5:19]+file_extension)
    os.rename(filename, newname)


#_____________________________________________________________________
#_____________________________________________________________________
#Begin GIS Loop
#_____________________________________________________________________
#_____________________________________________________________________

#Imports

import arcpy
import os
import glob
from arcpy import env
from arcpy.sa import *

arcpy.CheckOutExtension("Spatial")

#_____________________________________________________________________

#Define Variables

env.workspace = r"File_Path_For_GIS_Project"
arcpy.env.extent = r"File_Path_For_Shapefile.shp"
```

```
indef_file = "File_Path_For_Classification_Scheme.ecd"


outpath = r"File_Path_For _Saved_EM_Files"
outpath2 = r"File_Path_For _Saved_CR_Files"
outpath3 = r"File_Path_For _Saved_CS_Files"
outpath4 = r"File_Path_For _Saved_Final_Output_Files"

inMaskData = "Basin_Quadrat_Name"
extraction_area = "OUTSIDE"
analysis_extent = "Basin_Quadrat_Name"

ImageFolder = r"Input_Image_Path"

#_____________________________________________________________________

# Set up Rasters for Loops

inRastersName = [f for f in os.listdir(ImageFolder) if
f.endswith(".tif")]

inRasters = glob.glob(r"Input_Image_Path\\*.tif")

#_____________________________________________________________________

#Loop 1

for inRaster in inRasters:
    print(inRaster)
    outExtractMask = ExtractByMask(inRaster,inMaskData)
    print(outExtractMask)
    outname = os.path.join(outpath,
os.path.basename(inRaster).split(".")[0]+ "_EM.tif")
    print(outname)
    outExtractMask.save(outname)

    classifiedraster = ClassifyRaster(outExtractMask,
indef_file)
    outname2 = os.path.join(outpath2,
os.path.basename(inRaster).split(".")[0]+ "_CR.tif")
    print(outname2)
    classifiedraster.save(outname2)

#_____________________________________________________________________

#Loop 2
```

```
inRasters2 = glob.glob(r"outpath2\\*.tif")

for inRaster2 in inRasters2:
    arcpy.env.parallelProcessingFactor = "70%"
    outCellStatistics = CellStatistics(inRaster2, "SUM", "DATA")
    outname3 = os.path.join(outpath3,
os.path.basename(inRaster2).split(".")[0]+ "_CS.tif")
    print(outname3)
    outCellStatistics.save(outname3)

    outExtractMask = ExtractByMask(outCellStatistics,inMaskData)
    print(outExtractMask)
    outname4 = os.path.join(outpath4,
os.path.basename(inRaster2).split(".")[0]+ "_FINAL.tif")
    print(outname4)
    outExtractMask.save(outname4)
```

Appendix B. Additional Figures

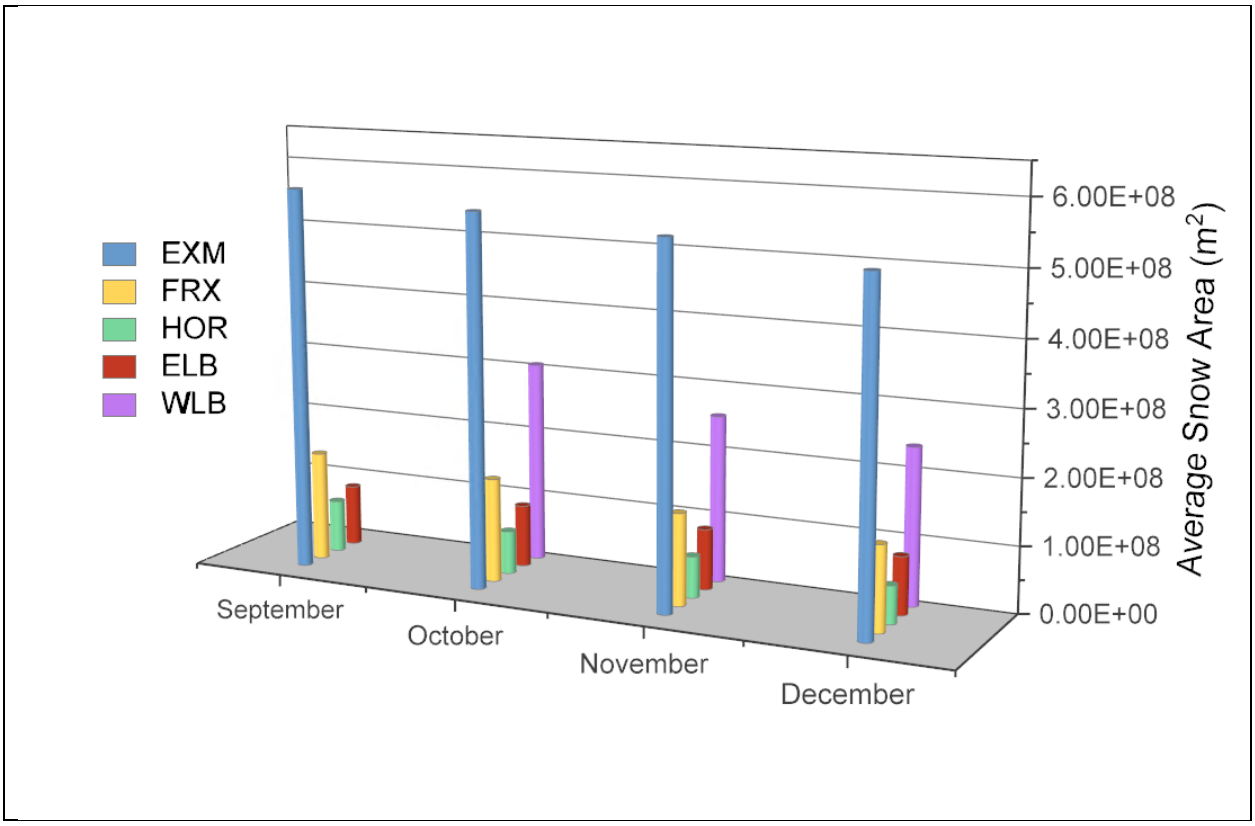

Figure B.1. The monthly snow coverage averages for each basin.

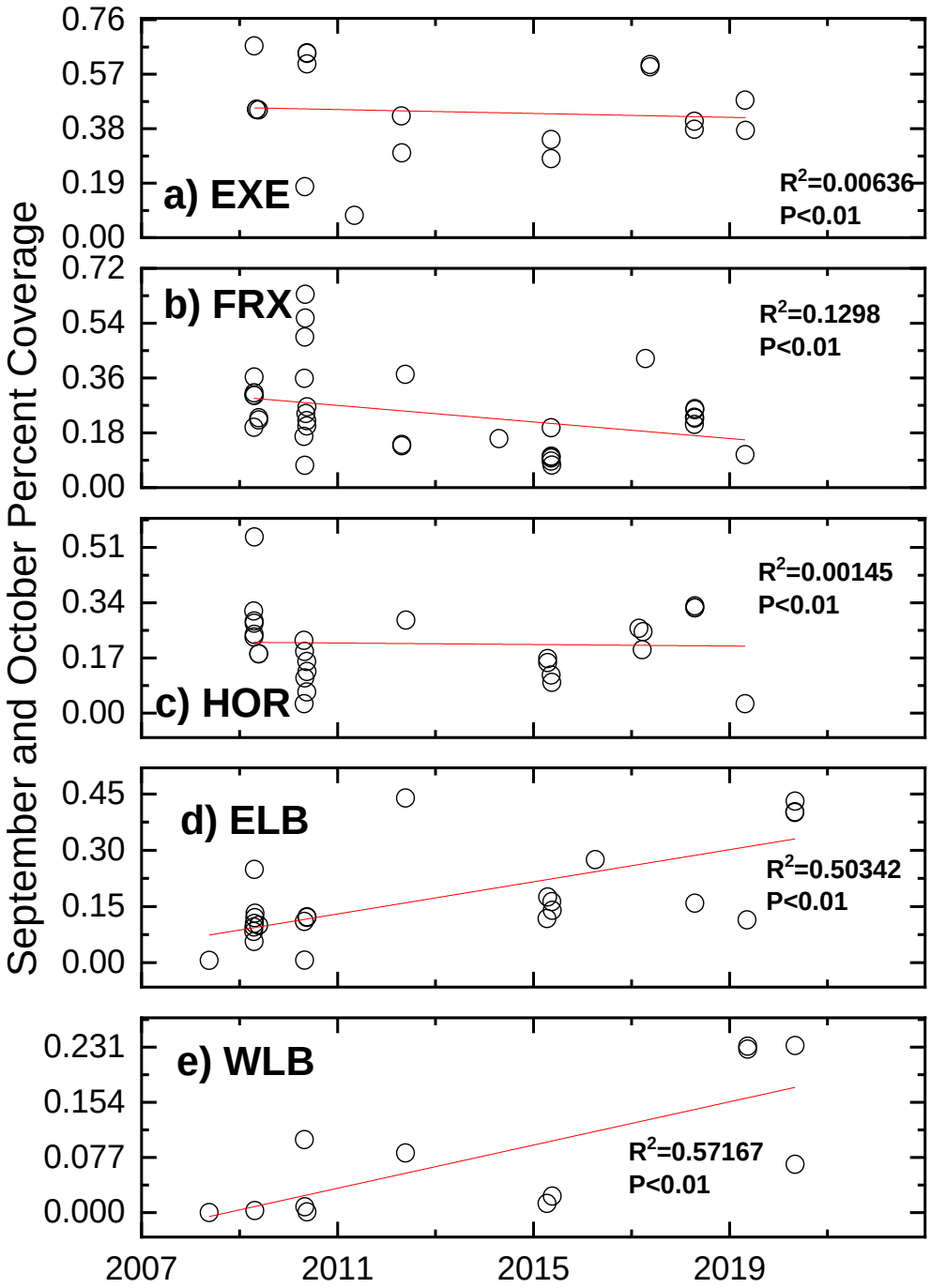

Figure B.2: Fractional coverage from the months September and October. A red trend line is applied to each basin dataset.

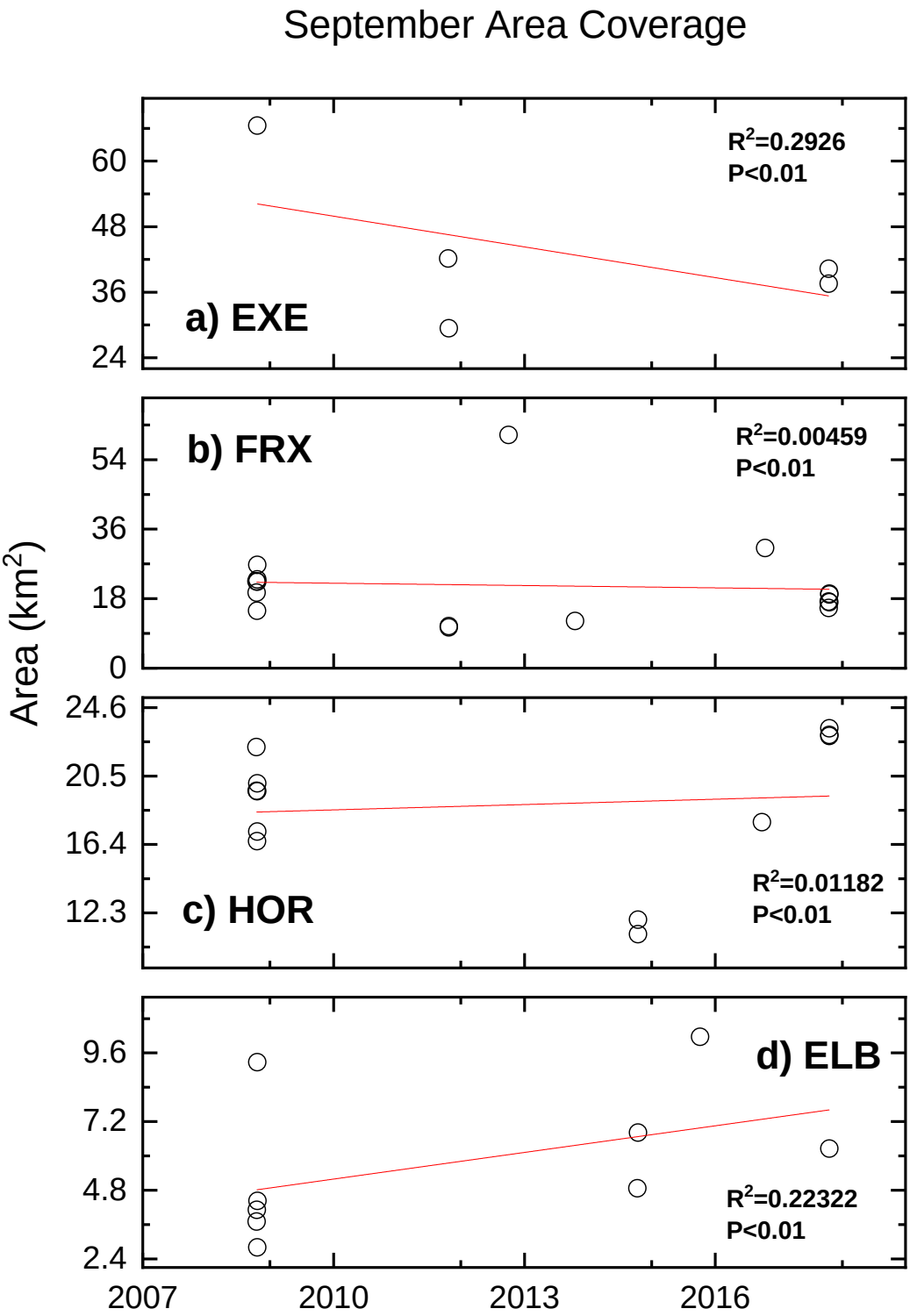

Figure B.3: September average area per basin.

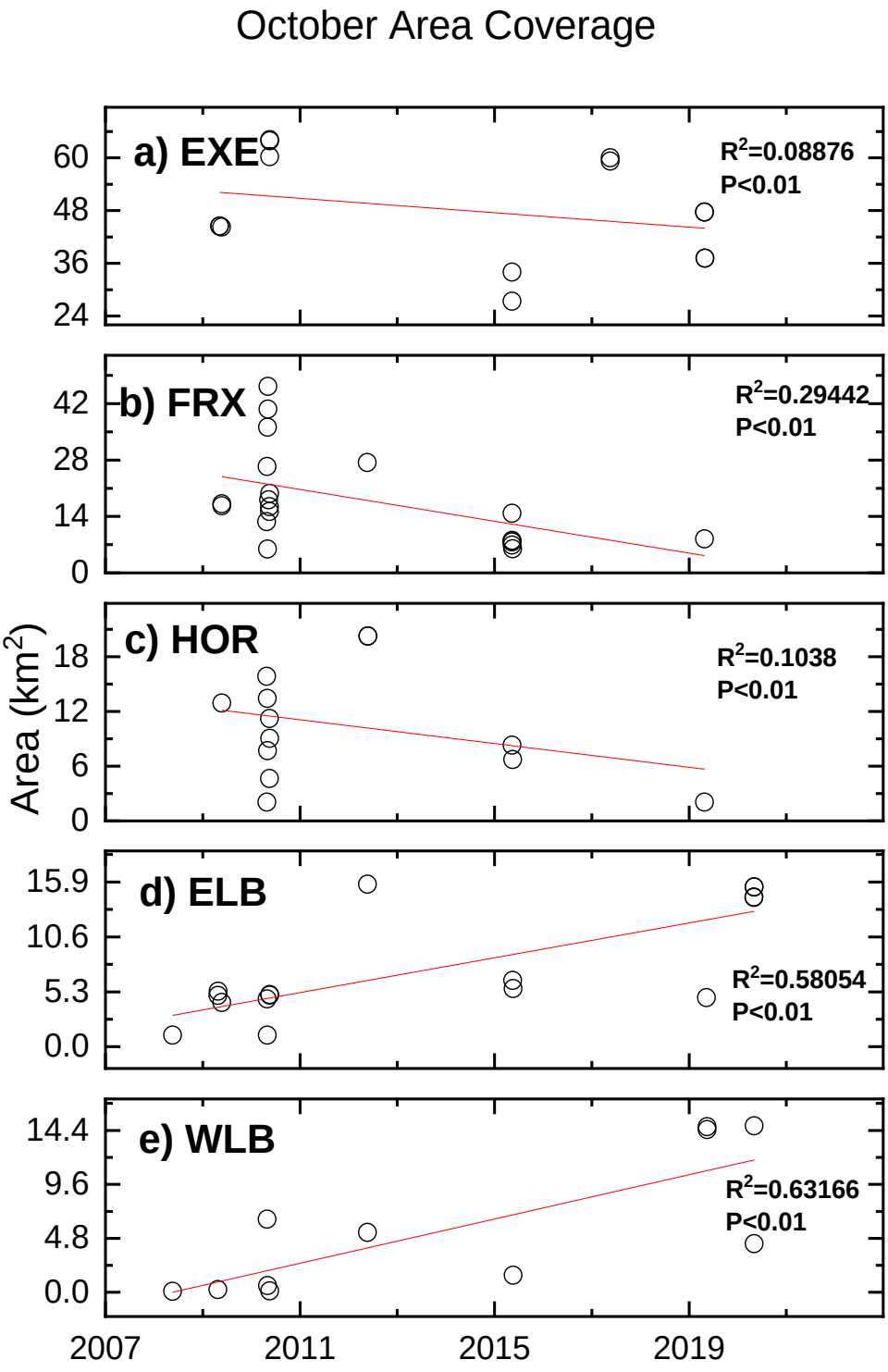

Figure B.4: October average area per basin.

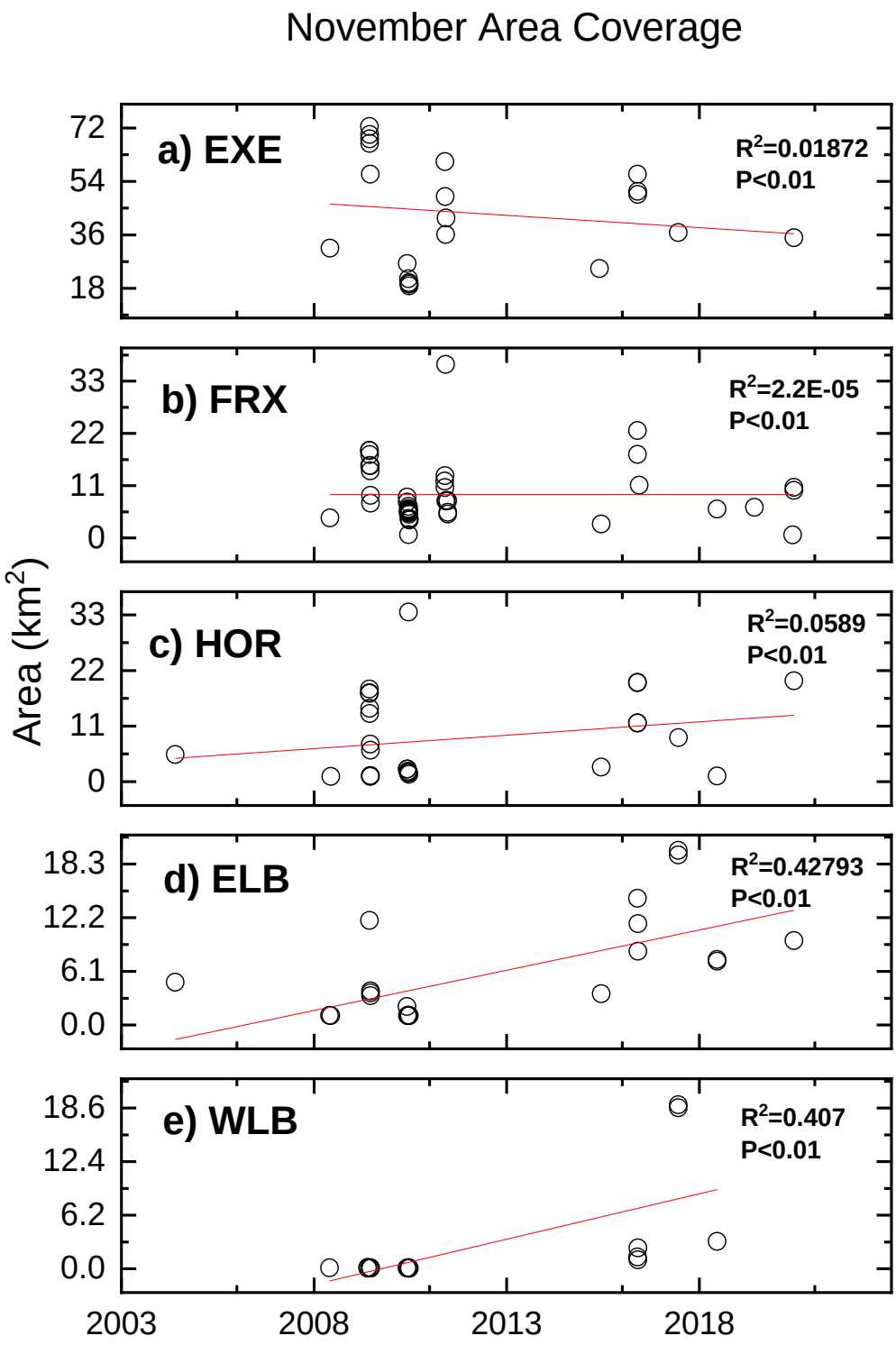

Figure B.5: November average area per basin.

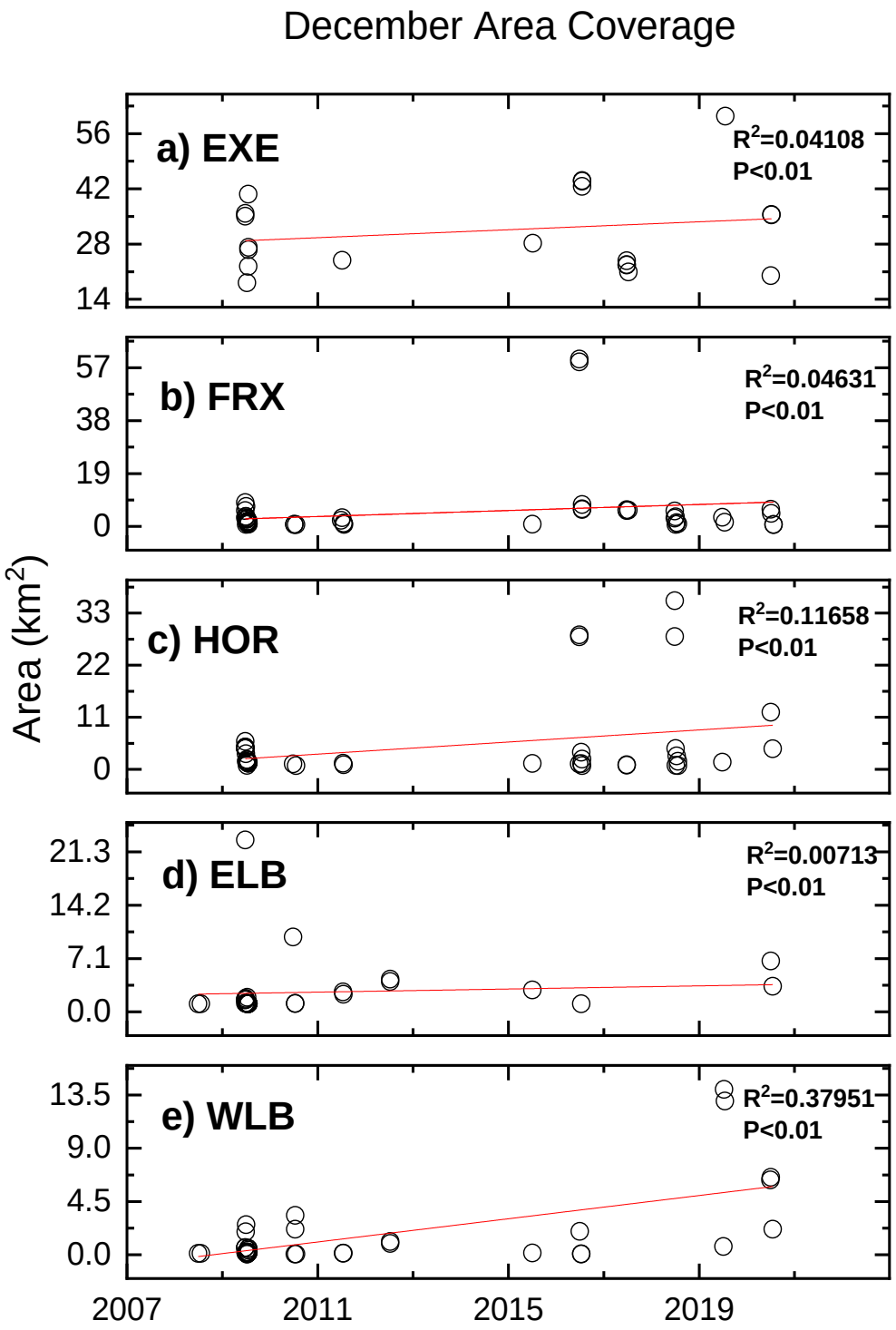

Figure B.6: December average area per basin.

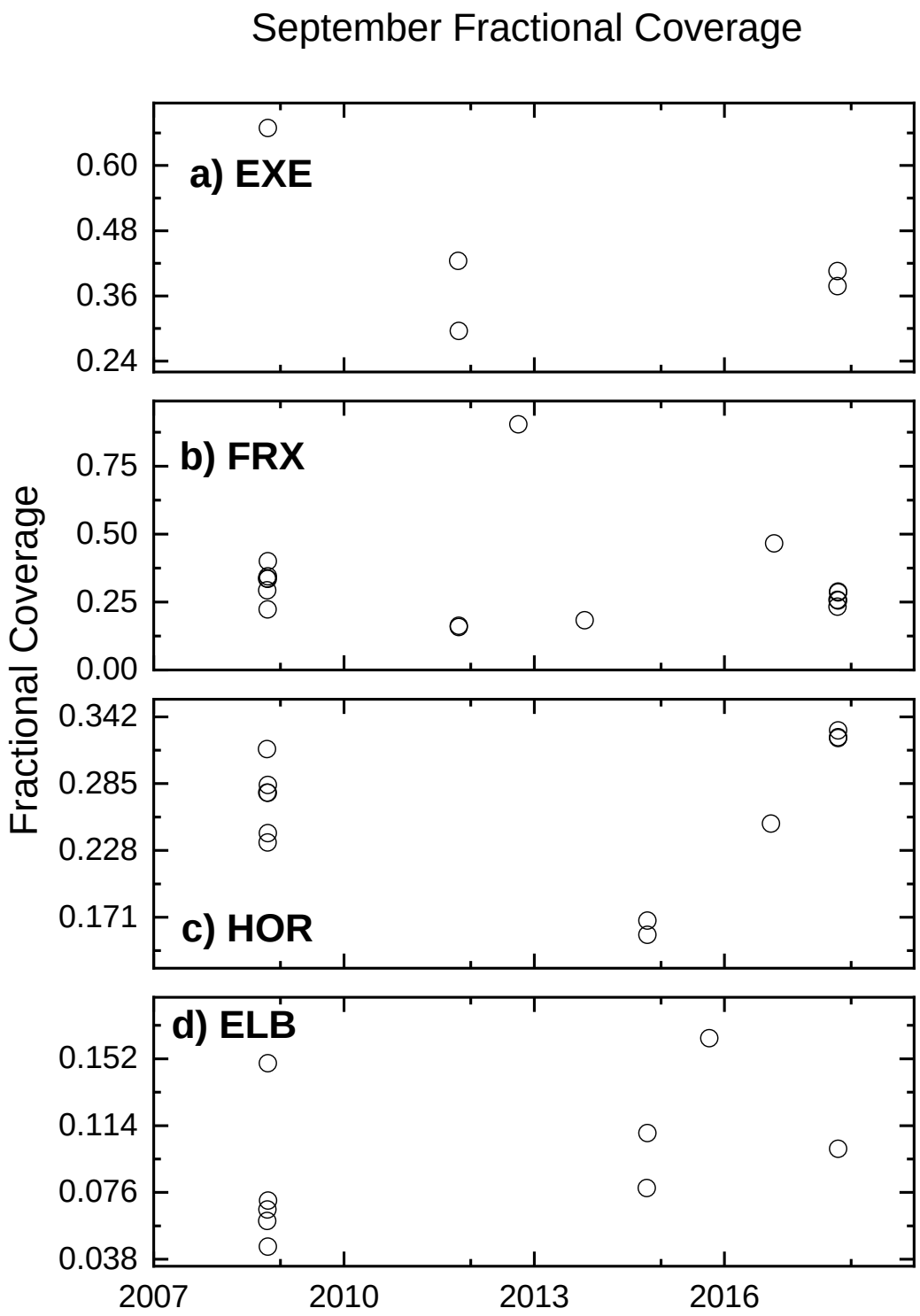

Figure B.7: September fractional coverage per basin.

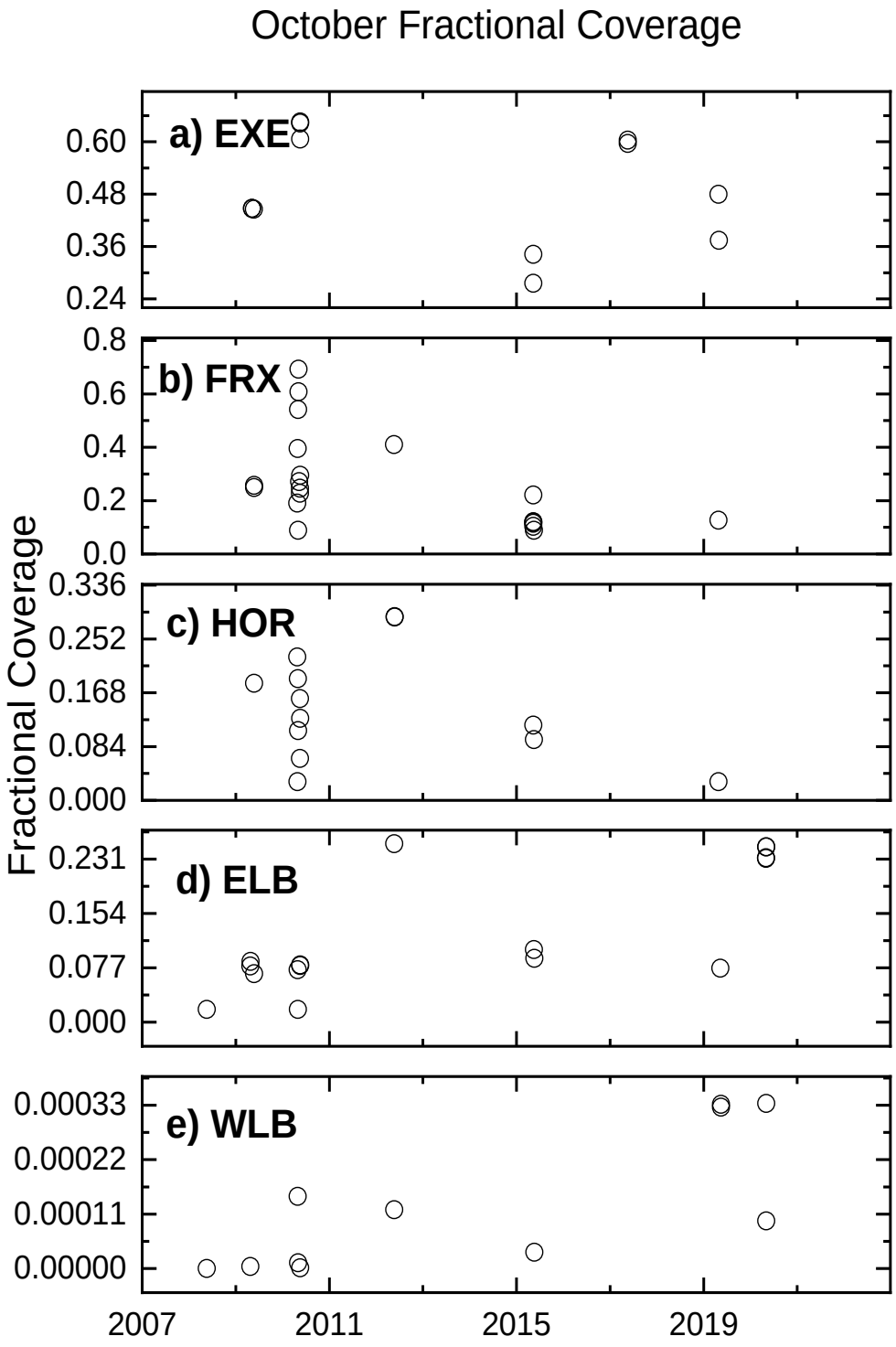

Figure B.8: October fractional coverage per basin.

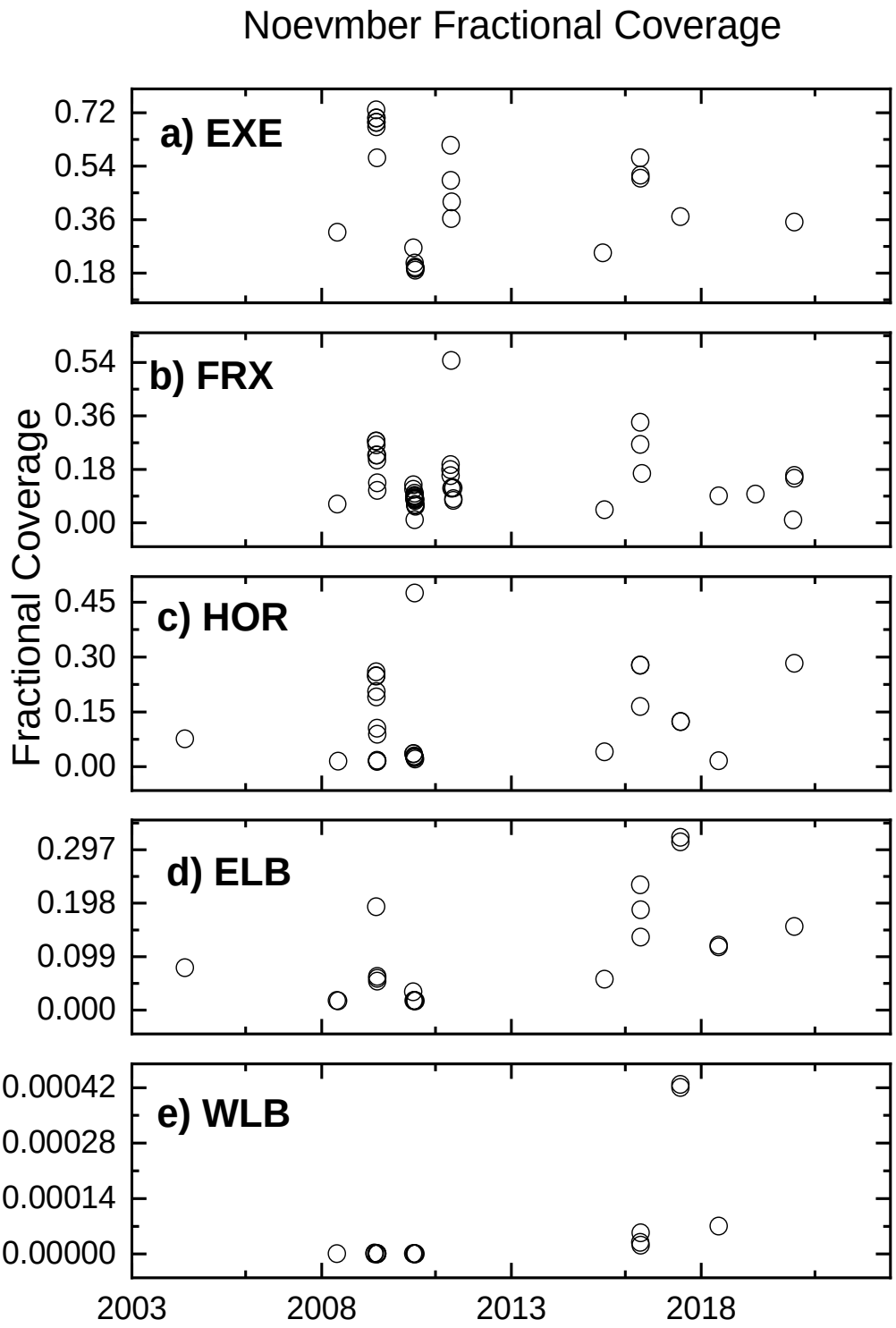

Figure B.9: November fractional coverage per basin.

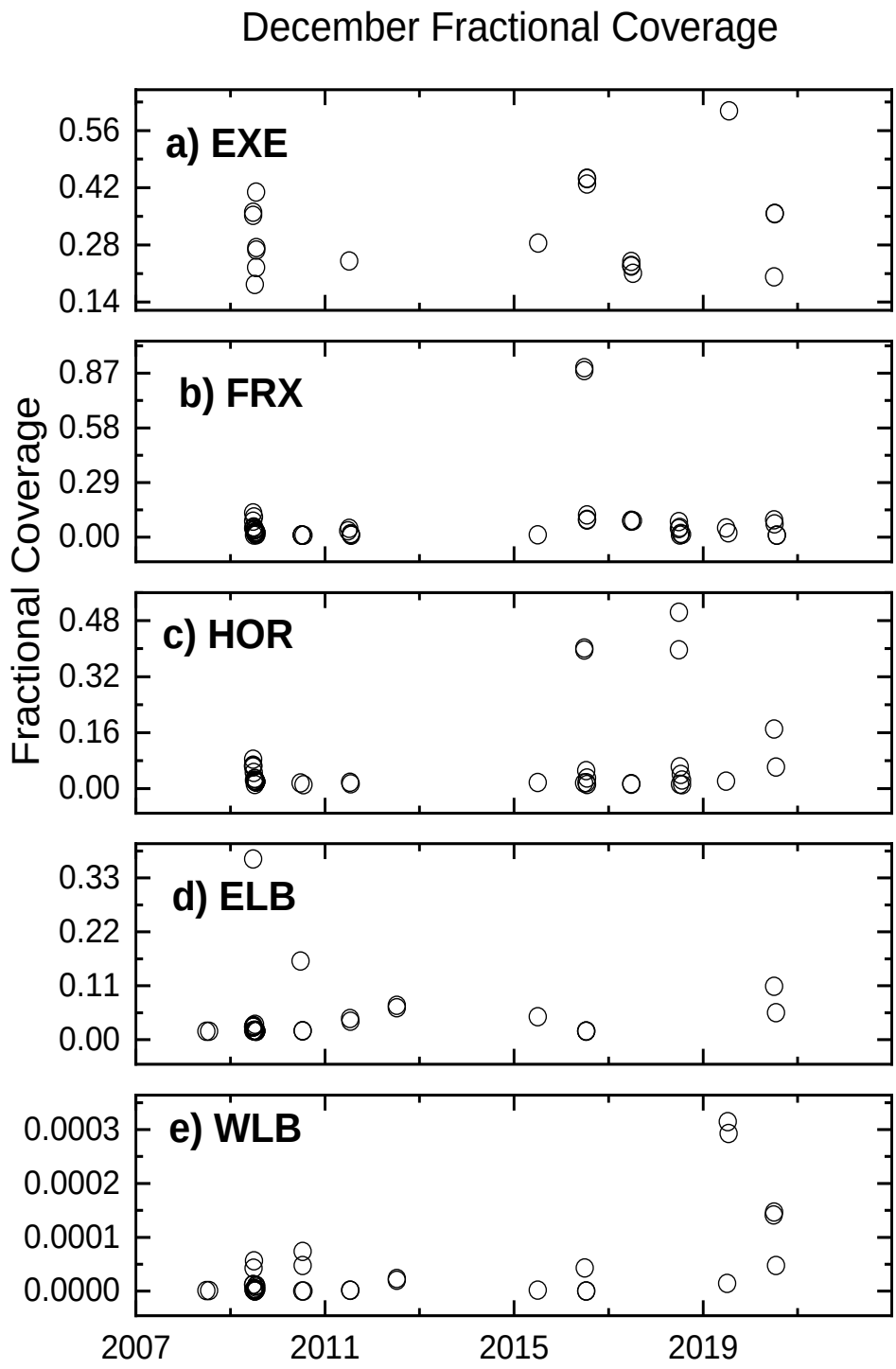

Figure B.10: December fractional coverage per basin.

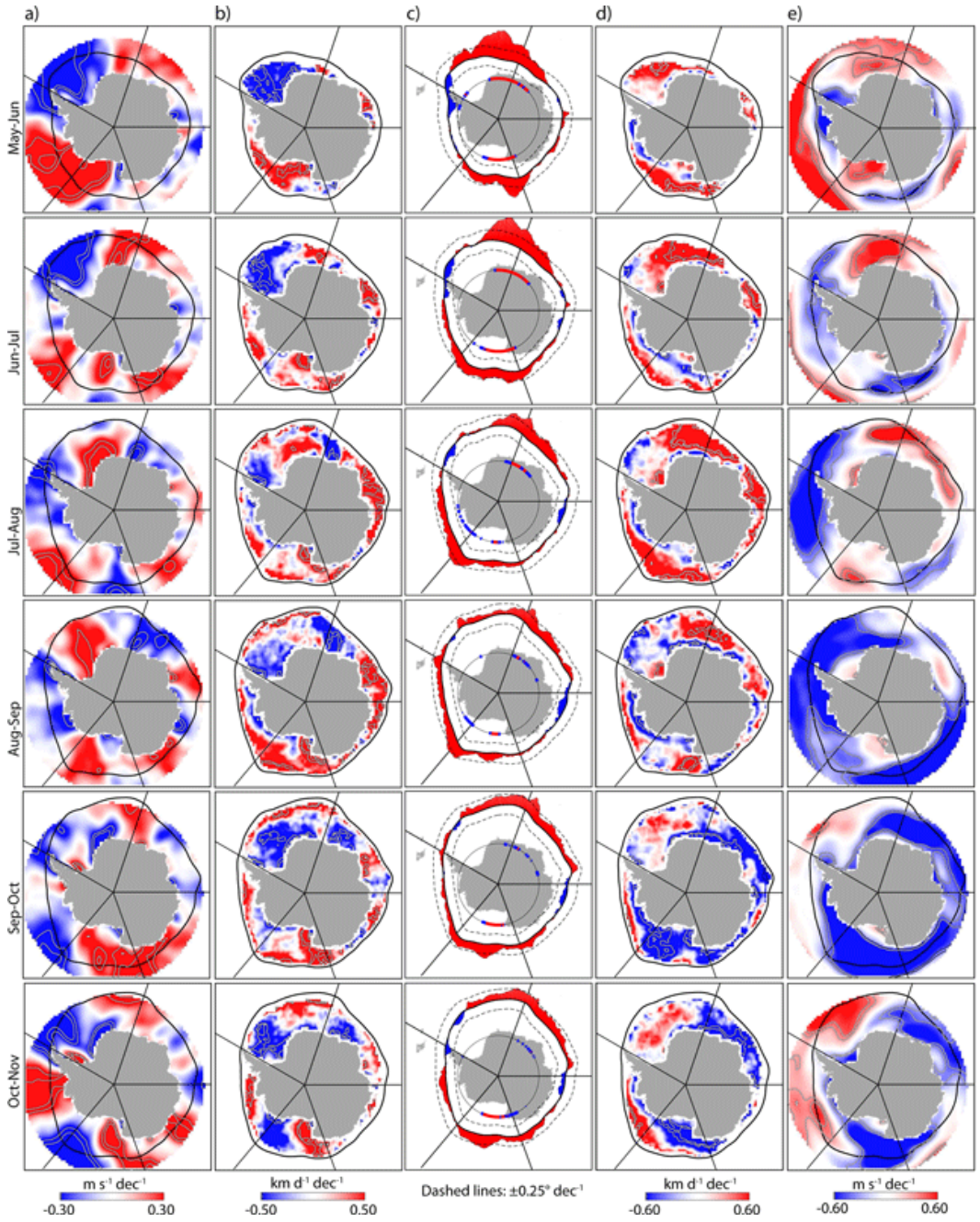

Figure B.11: "Trends (1982–2015) in wind, ice drift, and ice edge. (a) Meridional winds. (b) Meridional ice drift. (c) Ice edge. (d) Zonal ice drift. (e) Zonal winds. Trends in ice edge (in degrees of latitude per decade) are relative to the 2-month mean ice edge over the 34-year record (in black). Positive/negative ice edge trends are in red/blue. Also shown are the five geographic sectors typically used for calculation of trends in ice extent. Color of interior circles shows the confidence level in the ice edge trend (blue: > 95%, red: > 99%; black ≤ 95%). DOI: https://doi.org/10.1525/elementa.226.f5" From Kwok et al. (2017). In columns A and D, the changes in meridional winds and zonal ice drift can be observed from September to October.

References

ASTM D2216-19. 2019. Standard Test Methods for Laboratory Determination of Water (Moisture) Content of Soil and Rock by Mass, ASTM International, West Conshohocken, PA, www.astm.org.

Bergstrom, A., et al. 2020. "The seasonal evolution of albedo across glaciers and the surrounding landscape of Taylor Valley, Antarctica." The Cryosphere 14(3): 769-788.

Bertler, N. A. N., Barrett, P. J., Mayewski, P. A., Fogt, R. L., Kreutz, K. J., and Shulmeister, J. (2004), El Niño suppresses Antarctic warming, Geophys. Res. Lett., 31, L15207, doi:10.1029/2004GL020749.

Chinn, T. J. H. 1981. Hydrology and climate in the Ross Sea area. Journal of the Royal Society of New Zealand. 11(4): 373-386. DOI: 10.1080/03036758.1981.10423328.

Cohen, J., Ye, H., and Jones, J. 2015. Trends and variability in rain-on-snow events, Geophys. Res. Lett., 42, 7115– 7122, doi:10.1002/2015GL065320.

Dana, G.L., Wharton, R.A., Jr. and Dubayah, R.A. 1998. Solar Radiation in the Mcmurdo Dry Valleys, Antarctica. In Ecosystem Dynamics in a Polar Desert: the Mcmurdo Dry Valleys, Antarctica, J.C. Priscu (Ed.). https://doi.org/10.1029/AR072p0039.

Denton, G.H. and Marchant, D.R. 2000. The Geologic Basis for a Reconstruction of a Grounded Ice Sheet in McMurdo Sound, Antarctica, at the Last Glacial Maximum. Geografiska Annaler: Series A, Physical Geography, 82: 167-211. https://doi.org/10.1111/j.0435-3676.2000.00121.x.

Doran, P. T., McKay, C. P., Clow, G. D., Dana, G. L., Fountain, A. G., Nylen, T., and Lyons, W. B., 2002. Valley floor climate observations from the McMurdo dry valleys, Antarctica, 1986–2000, J. Geophys. Res., 107(D24), 4772, doi:10.1029/2001JD002045.

Doran, P. T., Priscu, J. C., Lyons, W. B., Walsh, J. E., Fountain, A. G., McKnight, D. M., Moorhead, D. L., Virginia, R. A., Wall, D. H., Clow, G. D., Fritsen, C. H., McKay, C. P., and Parsons, A. N. 2002. Antarctic climate cooling and terrestrial ecosystem response. Nature, 415(6871), 517–520. https://doi.org/10.1038/nature710.

Eveland, J. W., Gooseff, M. N., Lampkin, D. J., Barrett, J. E., and Takacs-Vesbach, C. D.: 2013. Seasonal controls on snow distribution and aerial ablation at the snow-patch and landscape scales, McMurdo Dry Valleys, Antarctica, The Cryosphere, 7, 917–931, https://doi.org/10.5194/tc-7-917-2013.

Fountain, A.G., Dana, G.L., Lewis, K.J., Vaughn, B.H. and Mcknight, D.H. 1998. Glaciers of the Mcmurdo Dry Valleys, Southern Victoria Land, Antarctica. In Ecosystem Dynamics in a Polar Desert: the Mcmurdo Dry Valleys, Antarctica, J.C. Priscu (Ed.). https://doi.org/10.1029/AR072p0065.

Fountain, A. G, Lyons W.B., Burkins M.B., Dana G.L., Doran P.T., Lewis K.J., McKnight D.M., Moorhead D.L., Parsons A.N., Priscu J.C, Wall D.H., and Wharton R.A.,, Virginia, R.A. 1999. Physical Controls on the Taylor Valley Ecosystem, Antarctica. BioScience. 49(12): 961-971. DOI: https://doi.org/10.1525/bisi.1999.49.12.961.

Fountain, A., Nylen, T., MacClune, K., and Dana, G. 2006. Glacier mass balances (1993-2001), Taylor Valley, McMurdo Dry Valleys, Antarctica. Journal of Glaciology. 52: 451-462. DOI: 10.3189/172756506781828511.

Fountain, A.G., Nylen, T.H., Monaghan, A., Basagic, H.J. and Bromwich, D. 2010. Snow in the McMurdo Dry Valleys, Antarctica. Int. J. Climatol., 30: 633-642. https://doi.org/10.1002/joc.1933.

Fountain, A. G., Fernandez-Diaz, J. C., Obryk, M., Levy, J., Gooseff, M., Van Horn, D. J., Morin, P., and Shrestha, R. 2010. High-resolution elevation mapping of the McMurdo Dry Valleys, Antarctica, and surrounding regions, Earth Syst. Sci. Data, 9, 435-443, https://doi.org/10.5194/essd-9-435-2017.

Hagedorn, B., Sletten, R. S., and Hallet, B. 2007. Sublimation and ice condensation in hyperarid soils: Modeling results using field data from Victoria Valley, Antarctica, J. Geophys. Res., 112, F03017, doi:10.1029/2006JF000580.

Harris, K.J., Carey, A.E., Lyons, W.B., Welch, K.A., and Fountain, A.G. 2007. Solute isotope geochemistry of subsurface ice melt seeps in Taylor Valley, Antarctica. GSA Bulletin 119: 548–555.

Heymsfield, A. J., A. Bansemer, A. Theis, and C. Schmitt. 2021. Survival of Snow in the Melting Layer: Relative Humidity Influence. J. Atmos. Sci., 78, 1823–1845, https://doi.org/10.1175/JAS-D-20-0353.1.

Kimura, N. 2007. Mechanisms controlling the temporal variation of the sea ice edge in the Southern Ocean. J Oceanogr. 63, 685–694, Retrieved from https://doi.org/10.1007/s10872-007-0060-3.

Kwok, R., Pang, S., and Kacimi, S. 2017. Sea ice drift in the Southern Ocean: Regional patterns, variability, and trends. Elementa: Science of the Anthropocene, 5 32. doi: https://doi.org/10.1525/elementa.226

Levy, J. 2013. How big are the McMurdo Dry Valleys? Estimating ice-free area using Landsat image data. Antarctic Science, 25(1), 119-120. Retrieved from https://doi.org/10.1017/S0954102012000727.

Li, L., and Pomeroy, J. W. 1997. Probability of occurrence of blowing snow, *J. Geophys. Res.*, 102(D18), 21955– 21964, doi:10.1029/97JD01522.

McKay, C., Mellon, M., and Friedmann, E. 1998. Soil temperatures and stability of ice-cemented ground in the McMurdo Dry Valleys, Antarctica. Antarctic science, 10 1, 31-8. DOI: 10.1017/S0954102098000054.

McKnight, D. M., Niyogi, K., Alger A., Bomblies, A., Conovitz, P., and Tate, C. 1999. Dry Valley Streams in Antarctica: Ecosystems Waiting for Water. BioScience .49(12): 985-995. DOI: 10.1525/bisi.1999.49.12.985.

McMurdo Dry Valleys Long Term Ecological Research program (OPP-1637708). https://mcm.lternet.edu.

Myers, M.E., 2019. Spatiotemporal Impact of Snow on Underwater Photosynthetically Active Radiation in Taylor Valley, East Antarctica. LSU Master's Theses. 4965.https://digitalcommons.lsu.edu/gradschool_theses/4965.

Myers, M. E., Doran, P. T., and Myers, K. F. 2020. Summer valley-floor snowfall in Taylor Valley, Antarctica from 1995–2017, The Cryosphere Discuss. [preprint], https://doi.org/10.5194/tc-2020-203.

Myers, K. F. 2018. Groundwater and thermal legacy of a large paleolake in Taylor Valley, East Antarctica as evidenced by airborne electromagnetic and sedimentological techniques. (M.S.). Louisiana State University, Baton Rouge, LA. Retrieved from https://digitalcommons.lsu.edu/gradschool_theses/4776.

Nylen, T. H., Fountain, A. G., and Doran, P. T. 2004, Climatology of katabatic winds in the McMurdo dry valleys, southern Victoria Land, Antarctica, J. Geophys. Res., 109, D03114, doi:10.1029/2003JD003937.

Obryk, M. K., Doran, P. T., Fountain, A. G., Myers, M., and McKay, C. P. 2020. Climate from the McMurdo Dry Valleys, Antarctica, 1986–2017: Surface air temperature trends and redefined summer season. Journal of Geophysical Research: Atmospheres, 125, e2019JD032180. https://doi.org/10.1029/2019JD032180.

Patterson, N., Bertler, N., Naish, T., and Morgenstern, U. 2005. ENSO variability in the deuterium-excess record of a coastal Antarctic ice core from the McMurdo Dry Valleys, Victoria Land. Annals of Glaciology, 41, 140-146. Doi:10.3189/172756405781813339

Powers J.G., Monaghan A.J., Cayette A.M., Bromwich D.H., Kuo Y.H., and Manning K.W. 2003. Real-time mesoscale modeling over Antarctica: The Antarctic Mesoscale Prediction System (AMPS). Bulletin of the American Meteorological Society. 84: 1533–154.

Price, M. 2020. Mastering ArcGIS Pro. McGraw Hill. E1. ISBN10: 1260587339.

Sugden, D., Marchant, D., Potter, Souchez, R., Denton, G., Swisher C., and Tison, J.L. 1995. Preservation of Miocene glacier ice in East Antarctica. Nature. 376, 412–414. Retrieved from https://doi.org/10.1038/376412a0.

Speirs, J.C., McGowan, H.A., Steinhoff, D.F. and Bromwich, D.H. 2013, Regional climate variability driven by foehn winds in the McMurdo Dry Valleys, Antarctica. Int. J. Climatol., 33: 945-958. https://doi.org/10.1002/joc.3481.

Stuiver M., Yang I.C., Denton G.H., and Kellog T.B. 1981. Antarctic Research Series: Dry Valley Drilling Project, McGinnis LD (ed) American Geophysical Union: Washington, DC; 131–139.

Sugden D.E., Marchant D.R., Potter N., Souchez R.A., Denton G.H., Swisher C.C., and Tison J.L. (1995). Preservation of Miocene Glacier Ice in East Antarctica. Nature. 376: 412–414. DOI: 10.1038/376412a0.

USDA and USSL Staff. 1954. Diagnosis and improvement of saline and alkali soils. USDA Handbook No 60 Washington DC, USA, 160 pp.

USGS. 2015. Standard Operating Procedure for Collection of Soil and Sediment Samples for the Sediment bound Contaminant Resiliency and Response (SCoRR) Strategy Pilot Study.: U.S. Geological Survey Open-File Report 2015–1188b, 37 p., http://dx.doi.org/10.3133/ofr20151188B.

Vignon, É., Roussel, M.L., Gorodetskaya, I. V., Genthon, C., and Berne, A. 2021. Present and future of rainfall in Antarctica. Geophysical Research Letters, 48, e2020GL092281. https://doi.org/10.1029/2020GL092281.

Wang, F. 2015. Quantitative Methods and Applications in GIS. Boca Raton, FL: CRC Press. ISBN 978-1-4665-8472-3.

Vita

Katie McNulty received her Bachelor of Science in Geology and Environmental Studies at the University of Cincinnati in 2016. While an undergraduate student, Katie was involved in projects focused on glacial lacustrine cores, stable-isotope geochemistry, glacial dynamics, and permafrost. After receiving her bachelor's degree, Katie worked in environmental consulting where she advanced her skillset in hydrology, vapor intrusion processes, remediation design, and hazardous waste management. Katie decided to pursue her master's degree at Louisiana State University to return to polar and cryosphere research. Through her research, Katie gained knowledge in Antarctic science and snow science, and gained skills in Geographic Information Systems (GIS) and Python. She plans to receive her Masters May 2023. After graduation from LSU Katie will work as a hydrogeologist for the Department of Ecology for Washington state.